WL-TR-96-2128

THERMAL MANAGEMENT RESEARCH STUDIES VOLUME 3 - HEAT PIPE IN HIGH-G ENVIRONMENT: ANALYSIS, DESIGN AND TESTING

Rengasamy Ponnappan, Ph.D.
UES, Inc.
4401 Dayton-Xenia Road
Dayton, OH 45432-1894

11 September 1996

Final Report for the period: March 1991 - September 1992

Approved for Public Release; Distribution is Unlimited.

AERO PROPULSION AND POWER DIRECTORATE
WRIGHT LABORATORY
AIR FORCE MATERIEL COMMAND
WRIGHT-PATTERSON AIR FORCE BASE, OH 45433-7251

NOTICE

USING GOVERNMENT DRAWINGS, SPECIFICATIONS, OR OTHER DATA INCLUDED IN THIS DOCUMENT FOR ANY PURPOSE OTHER THAN GOVERNMENT PROCUREMENT DOES NOT IN ANY WAY OBLIGATE THE US GOVERNMENT. THE FACT THAT THE GOVERNMENT FORMULATED OR SUPPLIED THE DRAWINGS, SPECIFICATIONS, OR OTHER DATA DOES NOT LICENSE THE HOLDER OR ANY OTHER PERSON OR CORPORATION; OR CONVEY ANY RIGHTS OR PERMISSION TO MANUFACTURE, USE, OR SELL ANY PATENTED INVENTION THAT MAY RELATE TO THEM.

THIS REPORT IS RELEASABLE TO THE NATIONAL TECHNICAL INFORMATION SERVICE (NTIS). AT NTIS, IT WILL BE AVAILABLE TO THE GENERAL PUBLIC, INCLUDING FOREIGN NATIONS.

THIS TECHNICAL REPORT HAS BEEN REVIEWED AND IS APPROVED FOR PUBLICATION.

JOHN E. LELAND
Project Engineer
Mechanical Branch

PHILLIP G. COLEGROVE
Technical Specialist
Mechanical Branch

MICHAEL A MARCINIAK, Major, USAF
Deputy Chief
Aerospace Power Division
Aero Propulsion and Power Directorate

IF YOUR ADDRESS HAS CHANGED, IF YOU WISH TO BE REMOVED FROM OUR MAILING LIST, OR IF THE ADDRESSEE IS NO LONGER EMPLOYED BY YOUR ORGANIZATION PLEASE NOTIFY WL/POSL, WRIGHT-PATTERSON AFB OH 45433-7103 TO HELP MAINTAIN A CURRENT MAILING LIST.

Do not return copies of this report unless contractual obligations or notice on a specific document requires its return.

REPORT DOCUMENTATION PAGE

Form Approved
OMB No. 0704-0188

1. AGENCY USE ONLY *(Leave blank)*

2. REPORT DATE
11 September 1996

3. REPORT TYPE AND DATES COVERED
Final March 1991 - September 1992

4. TITLE AND SUBTITLE
Thermal Management Research Studies Volume 3 -
HEAT PIPE IN HIGH-G ENVIRONMENT: ANALYSIS, DESIGN AND TESTING

5. FUNDING NUMBERS
C F33615-91-C-2104
PE-62203F
PR-3145
TA-20
WU-00

6. AUTHOR(S)
Rengasamy Ponnappan, Ph.D.

7. PERFORMING ORGANIZATION NAME(S) AND ADDRESS(ES)
UES, Inc.
4401 Dayton-Xenia Road
Dayton, OH 45432-1894

8. PERFORMING ORGANIZATION REPORT NUMBER
UES-255-TR-96-1
(Vol. 3)

9. SPONSORING/MONITORING AGENCY NAME(S) AND ADDRESS(ES)
Aero Propulsion and Power Directorate
Wright Laboratory
Air Force Materiel Command
Wright-Patterson AFB, OH 45433-7251
POC: John E. Leland, WL/POOS (937) 255-2922

10. SPONSORING/MONITORING AGENCY REPORT NUMBER
WL-TR-96-2128

11. SUPPLEMENTARY NOTES
The other volumes of this report are: Volume 1 - Electronics Cooling
Volume 2 - Rotating Heat Pipe

12a. DISTRIBUTION/AVAILABILITY STATEMENT
Approved for public release; distribution is unlimited

12b. DISTRIBUTION CODE

13. ABSTRACT *(Maximum 200 words)*

This report presents the details of a spin table test facility developed for testing heat pipes and other heat transfer experiments under high acceleration conditions. A drive system capable of variable spin up and spin down acceleration rates to simulate aircraft G-forces encountered during flight maneuvers is described. Also included are details on calorimetric testing, remote computer control operation and multichannel data acquisition capabilities of the spin table.

The effects of G-load on a heat pipe performance were analyzed with reference to the influence of bond number and operating temperature. The steady state test results of a flexible copper-water heat pipe under transverse accelerations up to 10G are presented along with those analytically predicted.

14. SUBJECT TERMS
Heat Pipe, Dynamic Environment, Spin Table, High "G" Acceleration, Bond Number, Actuator Cooling Application, Military Aircraft

15. NUMBER OF PAGES
57

16. PRICE CODE

17. SECURITY CLASSIFICATION OF REPORT	18. SECURITY CLASSIFICATION OF THIS PAGE	19. SECURITY CLASSIFICATION OF ABSTRACT	20. LIMITATION OF ABSTRACT
UNCLASSIFIED	UNCLASSIFIED	UNCLASSIFIED	SAR

NSN 7540-01-280-5500

Standard Form 298 (Rev. 2-89)
Prescribed by ANSI Std. Z39-18
298-102

TABLE OF CONTENTS

LIST OF ILLUSTRATIONS

LIST OF ILLUSTRATIONS (CONT'D.)

LIST OF TABLES

FOREWORD

This final technical report was prepared as part of the contract deliverables under the "Thermal Management Research" contract F33615-91-C-2104. This contract was sponsored and administered by the Aero Propulsion and Power Directorate (APPD) of Wright Laboratory (WL) at Wright-Patterson Air Force Base (WPAFB). Dr. J.E. Leland and Dr. K.L. Yerkes were the Air Force Project Engineers/Technical Monitors at various stages of the program.

The present volume (Volume 3) outlines the research effort performed under Task 002: High "G" Heat Transfer Study covering the spin table facility development at APPD's Thermal Laboratory and steady-state performance tests conducted on a flexible heat pipe. The other volumes of the final report are:

Volume 1: Electronics Cooling (Task 001)

Volume 2: Rotating Heat Pipe (Task 004)

The work described here was performed entirely on-site at the Thermal Laboratory (WL/POOS) by UES, Inc., Dayton, Ohio with Dr. R. Ponnappan as the Program Manager. Messrs. J. Tennant (UES), M.D. Ryan (UES) and D. Reinmuller (WL) provided the technical support. UES' Materials and Processes Division, together with the corporate publication group, provided the administrative and documentation support. The author sincerely appreciates the services by Dr. Qun He, UES, Inc., in preparing this document.

1.0 INTRODUCTION

1.1 BACKGROUND HISTORY

Heat pipes have a long history of dependable operation on the ground and in spacecraft applications where external forces are minimal.[1] In recent years, potential applications have been identified where heat pipes are subjected to vibration and acceleration body forces. Examples include the Navy's flexible heat pipe for aircraft actuator cooling [2], leading edge cooling of hypersonic airplanes and high power electronics cooling for the more electric airplane. High performance aircraft use sophisticated electronic equipment onboard. These electronic packages contain state-of-the-art high density circuit boards. Also, high power electro-mechanical actuators are used to activate the control surfaces of the aircraft. In order to maintain a proper thermal environment for these packages, some form of thermal management devices is built into the support structure. Future designs may use heat transfer systems such as heat pipes, two-phase pumped loop, immersion cooling, flow boiling devices, etc. It is important for the designer of the thermal systems to make sure that not only their thermal performance is met on the ground, but also during flight and maneuvers as well.[3] Aircraft electronic packages may undergo acceleration levels of 5 G (up to 7.3 G for short duration) with the vibration frequency ranging from 3 to 1000 Hz. Figure 1 shows a typical plot of acceleration vs. time profile for an F15 aircraft maneuver which forms the basis for simulation on a centrifuge table.[4] Table 1 shows the typical range of acceleration and frequency for various airborne and space vehicles.[3,5] However, these acceleration levels at high frequency range of vibration should not be confused with the low frequency acceleration levels of aircraft maneuvering shown in Figure 1.

The fundamental concern with the acceptance of a heat pipe for these applications is the understanding of this device under the induced external body forces. These forces are generated from a combination of random vibration and system acceleration. The forces may or may not be cyclic and occur in the adverse conditions with sufficient magnitude that they may easily deprime the wick structure and force restart scenarios. This problem is further complicated by the fact that the subsequent disturbance could occur prior to a completed restart. In order to evaluate these situations, a study has been initiated to investigate the heat pipe operation in an accelerating environment.

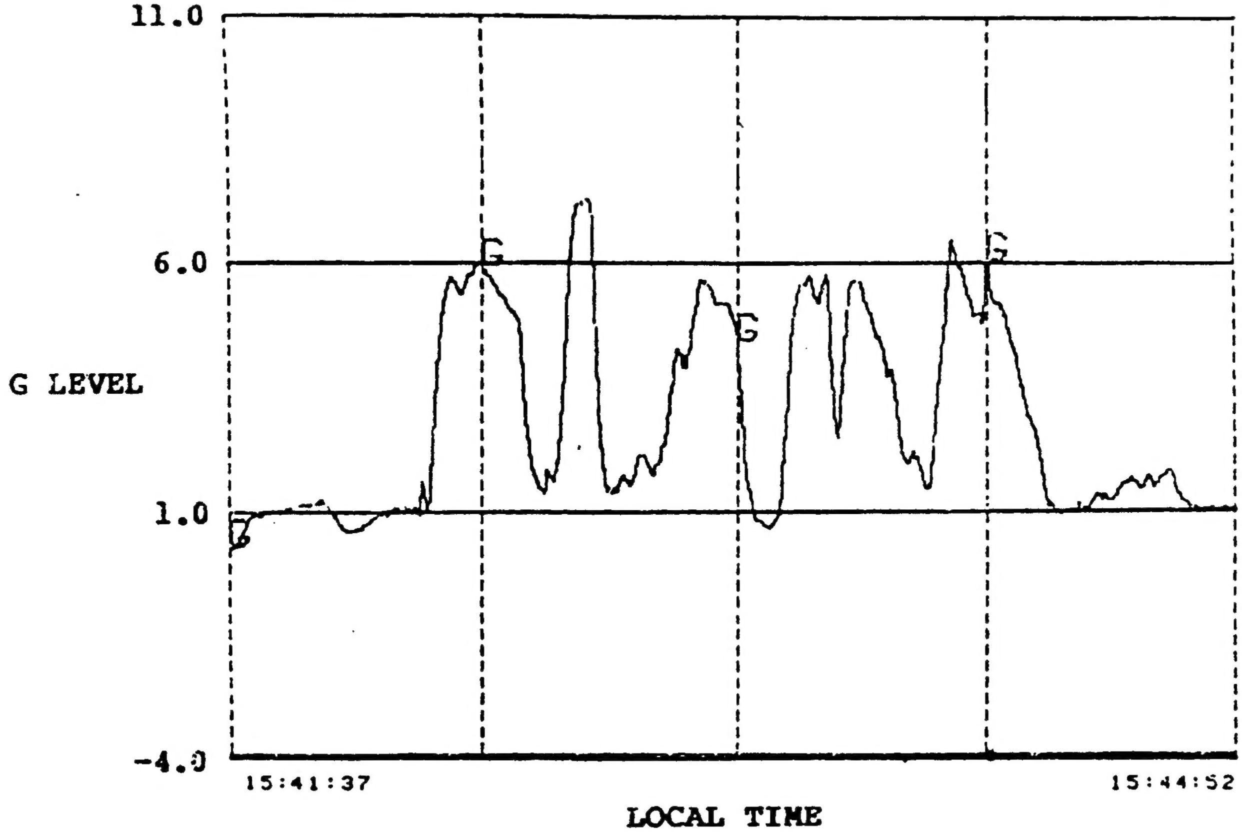

Figure 1. Typical Plot of G vs. Time for an F-15 Engagement, as Acquired Through the Air Combat Maneuvering Instrumentation System and the ACMI Data Plot Package. This Engagement Saw a Peak G Load of 7.3 G and a Maximum G-Onset Rate of 1.8 G/s. (Ref. 4)

Table 1. Vibration and Acceleration Levels of Electronic Equipment for Aircraft, Helicopter, and Aerospace Vehicles

Description	Vibration Frequency Spectrum	Acceleration
AIRCRAFT[3]		
Nominal range	3 - 1000 Hz	1 - 5 g (peak)
Highest Acceleration	100 - 400 Hz	5 g (in vertical direction)
Lowest Acceleration	100 - 400 Hz	1 g (in longitudinal direction)
HELICOPTERS[3]		
Nominal range	3 - 500 Hz	0.5 - 4 g
Higher Acceleration (NOTE: Very large displacements at low frequency: 5 mm at 10 Hz)	500 Hz	4 g (in vertical direction)
MISSILES[3]		
Nominal range	3 - 5000 Hz	5 - 30 g
Highest acceleration	>1000 Hz	30 g
SPACE SHUTTLE[5]		
Lateral Axis	20 - 2000 Hz	±6 g (each axis)
Longitudinal Axis	20 - 2000 Hz	±10 g

Note: These data are provided as a reference only. The influence of these high frequency vibration on heat transfer mechanisms would constitute an entirely different area of research and should not be interpreted as the low frequency, high-g maneuvering of aircraft that is addressed in this report.

Richardson et al. conducted tests on a stainless steel sinter wick heat pipe with simple harmonic vibration loads of 0-580 Hz and 0-12 G in the longitudinal direction and found that the heat transfer capacity dropped as the induced acceleration was increased.[6] Semena and Nikolaenko found that vibration loads (5-4000 Hz and 0.12-15 G) exert a significant effect on the thermal resistance and the transport capacity.[7] Hou and Wen analyzed the performance of a grooved heat pipe mounted on a spinning satellite.[8] They showed that an abrupt increase in heat pipe ΔT resulted at a threshold spin rate indicative of the evaporator dryout. Kiseev et al. investigated the performance of a heat pipe with separate liquid and vapor channels subjected to steady-state acceleration forces of 1-10 G.[9] They found that the heat pipe operated with a reduced maximum heat flux associated with a large thermal resistance when subjected to adverse acceleration forces.

1.2 SCOPE OF THE PRESENT STUDY

The scope of the present research was to:

- Analyze the effects of acceleration on the steady-state performance of heat pipes in order to understand the potential limitations and benefits of using such capillary devices under external body force environment;

- Design and develop a spin table test facility with adequate instrumentation and control; and

- Test a flexible heat pipe for performance under steady state transverse acceleration conditions and compare with theoretical predictions.

2.0 ANALYSIS

2.1 APPLICATION OF G-LOADS

2.1.1 Physical Orientation

The first step toward understanding the behavior of heat pipes under body force effects is to mount a test heat pipe on a horizontal centrifuge table at various orientations and test for performance. A few of the representative mounting arrangements are illustrated in Figure 2 and the favorable and unfavorable conditions for the heat pipe performance are indicated. The best and worst cases of available pumping head occurs in radial mounting, depending upon the relative positions of evaporator and condenser. In this case, under steady-state spin conditions, the induced acceleration is purely longitudinal in the heat pipe. The body forces developed due to this induced longitudinal acceleration will be in direct opposition with the surface tension forces in the wick for the case of evaporator end kept near the center of the table and vice versa (Figure 2, case I). On the other hand, the induced body forces are mostly in the transverse direction of the heat pipe for the cases of circumferential mounting as shown in cases II and III in

Mounting Orientation	Illustrative Sketch	Centrifugal Acceleration on Heat Pipe Sections	Remarks
I. Radial 1. Evaporator near center 2. Condenser near center	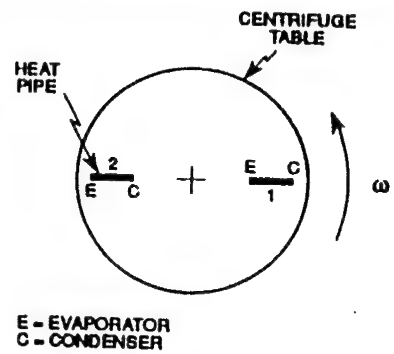	Nonuniform	1. G (radial) is unfavorable for liquid return 2. G (radial) is favorable for liquid return
II. Circumferential 1. Evaporator leading end 2. Condenser leading end	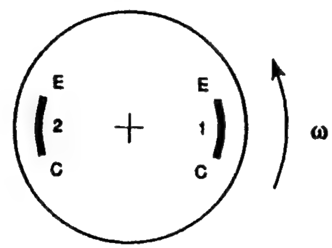	Uniform	1. G (tangential) is unfavorable 2. G (tangential) is favorable
III. Vertical 1. Evaporator over condenser 2. Condenser over evaporator	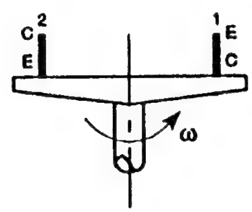	Uniform	1. Gravity opposed 2. Gravity assisted
IV. Flexible Heat Pipes 1,3 Evaporator leading end 2,4 Condenser leading end	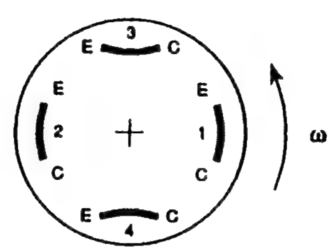	Nonuniform	1 & 2 Radial G is unfavorable for priming 3 & 4 Radial G is favorable 1 & 3 Tangential G is unfavorable 2 & 4 Tangential G is favorable

Figure 2. Heat Pipe Mounting Orientations for Spin Table Testing.

Figure 2. Straight heat pipes and flexible heat pipes with straight evaporator and condenser lengths cannot conform to a uniform radius of curvature and hence they will undergo nonuniform acceleration loads along their length.

The radial or centrifugal acceleration experienced by an object mounted at a radius, r, on a spin table rotating at a constant angular speed ω is given as

$$a_r = \omega^2 r = \left(\frac{2\pi N}{60}\right)^2 r \quad \textbf{(1)}$$

where N is the rotational speed in rpm.

If expressed in ratio of acceleration due to gravity "g" (= 9.81 m/s^2),

$$a_r = 1.1179 \times 10^{-3}\ N^2 r \quad \text{in G's} \quad \textbf{(2)}$$

This relation is graphically illustrated in Figure 3.

The tangential acceleration, $a_t = r\frac{d\omega}{dt}$ is not important for steady state analysis. Both induced tangential and vertical acceleration effects are not considered in this study for simplicity. Acceleration loads up to 10 G are easily created using a nominal spin rate of 100 rpm and radial arm of 1 m as indicated in Figure 3. By controlling the speed of the drive motor, various G-load profiles can be obtained. A typical simulated air combat maneuvering profile is shown in Figure 4 adapted from Reference 10.

2.1.2 <u>Flexible Heat Pipe</u>

The candidate heat pipe chosen for analysis and test is a flexible copper-water heat pipe fabricated by Thermacore for the U.S. Navy.[2] A detailed description and illustrations are included in Section 4.0, "Experimental Work." Additional details of the wicks and capillary performance limits of this heat pipe are given in the Appendix.

Figure 5 illustrates the top view of the circumferential mounting on a horizontal spin table. The acceleration component vectors and the adiabatic section arterial wick segment are shown in Figure 6.

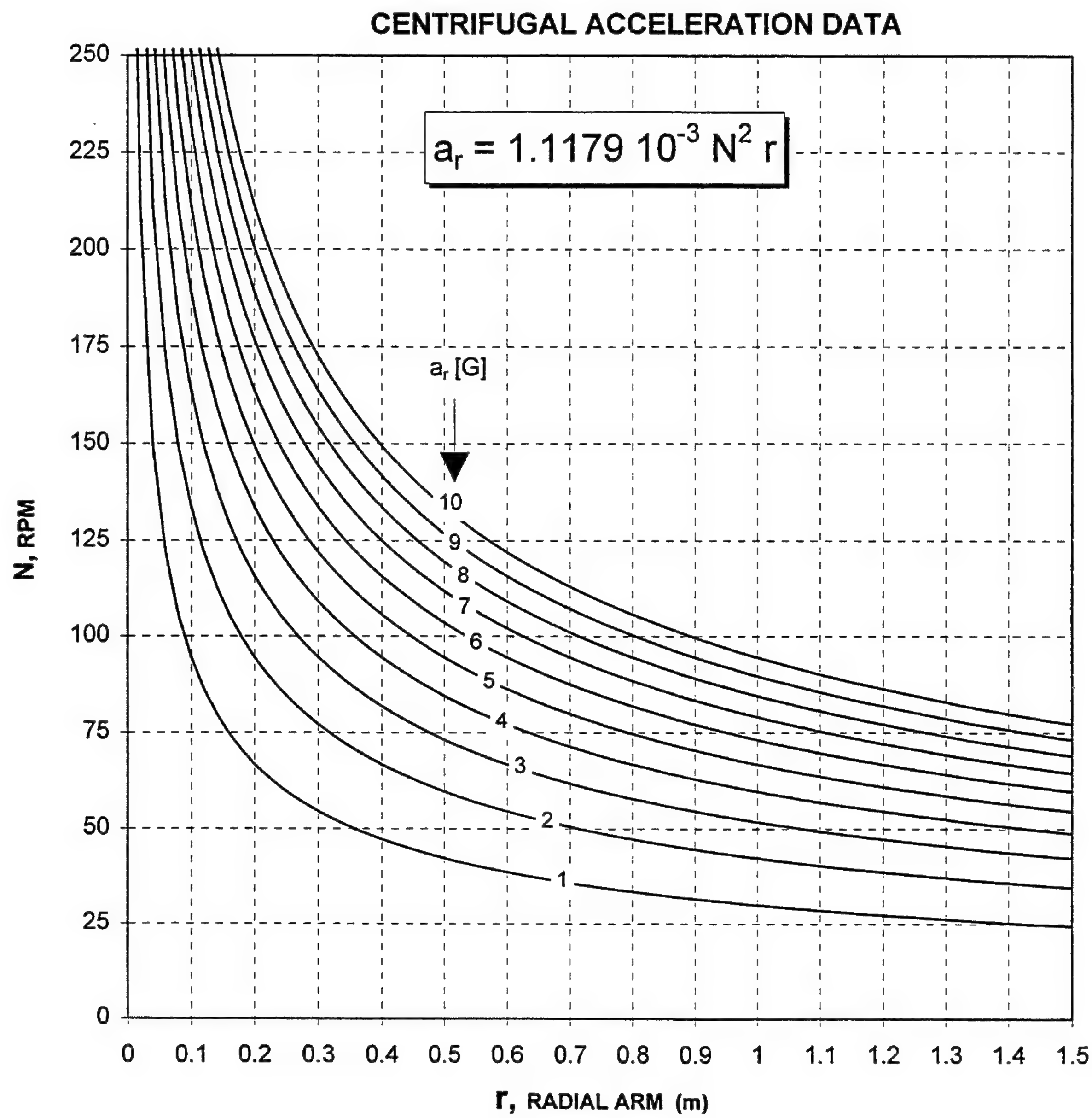

Figure 3. Centrifugal Acceleration Data as Functions of Table Spin Speed and Radial Arm Length.

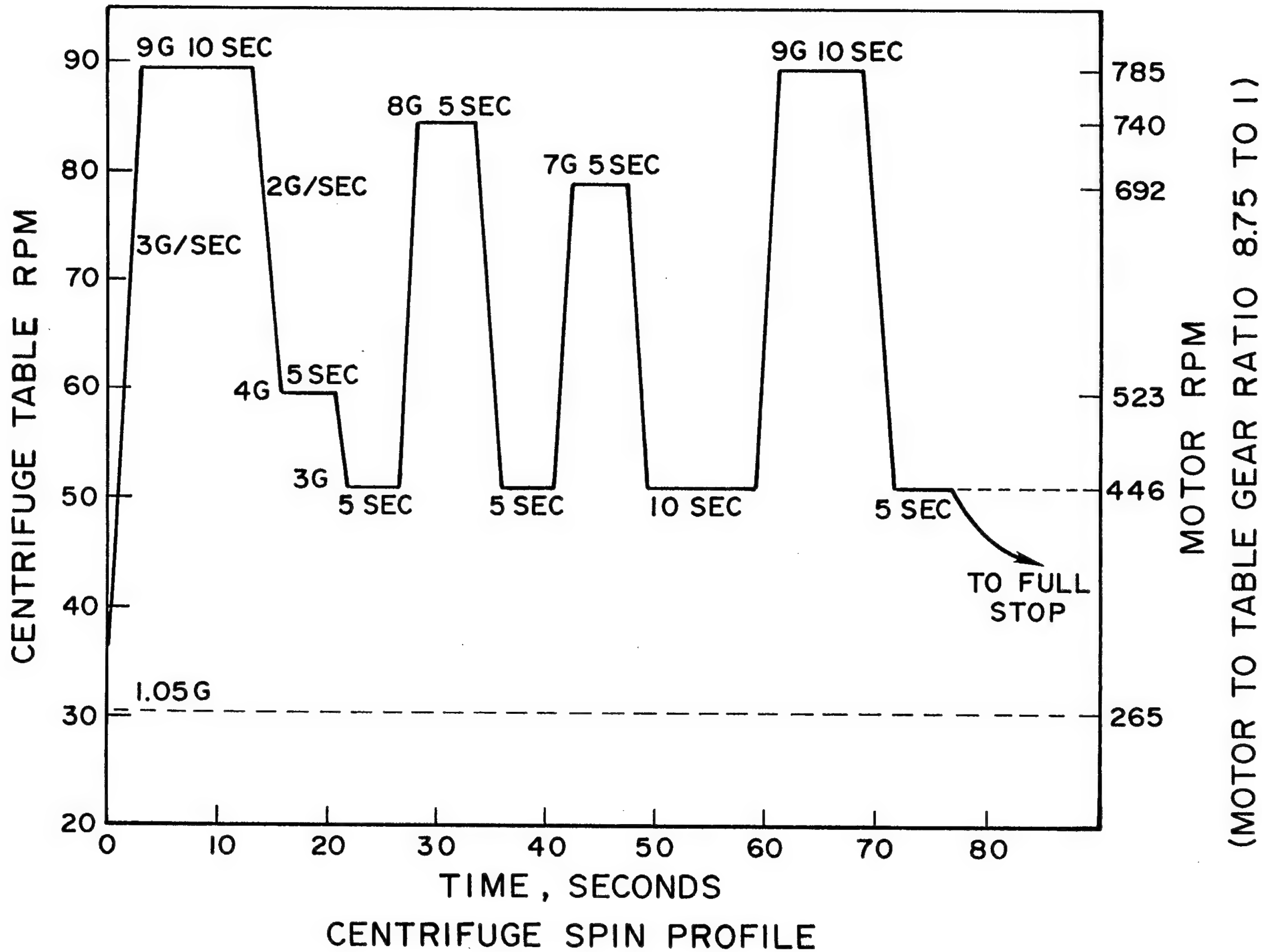

Figure 4. Simulated Air Combat Maneuvering Profile.

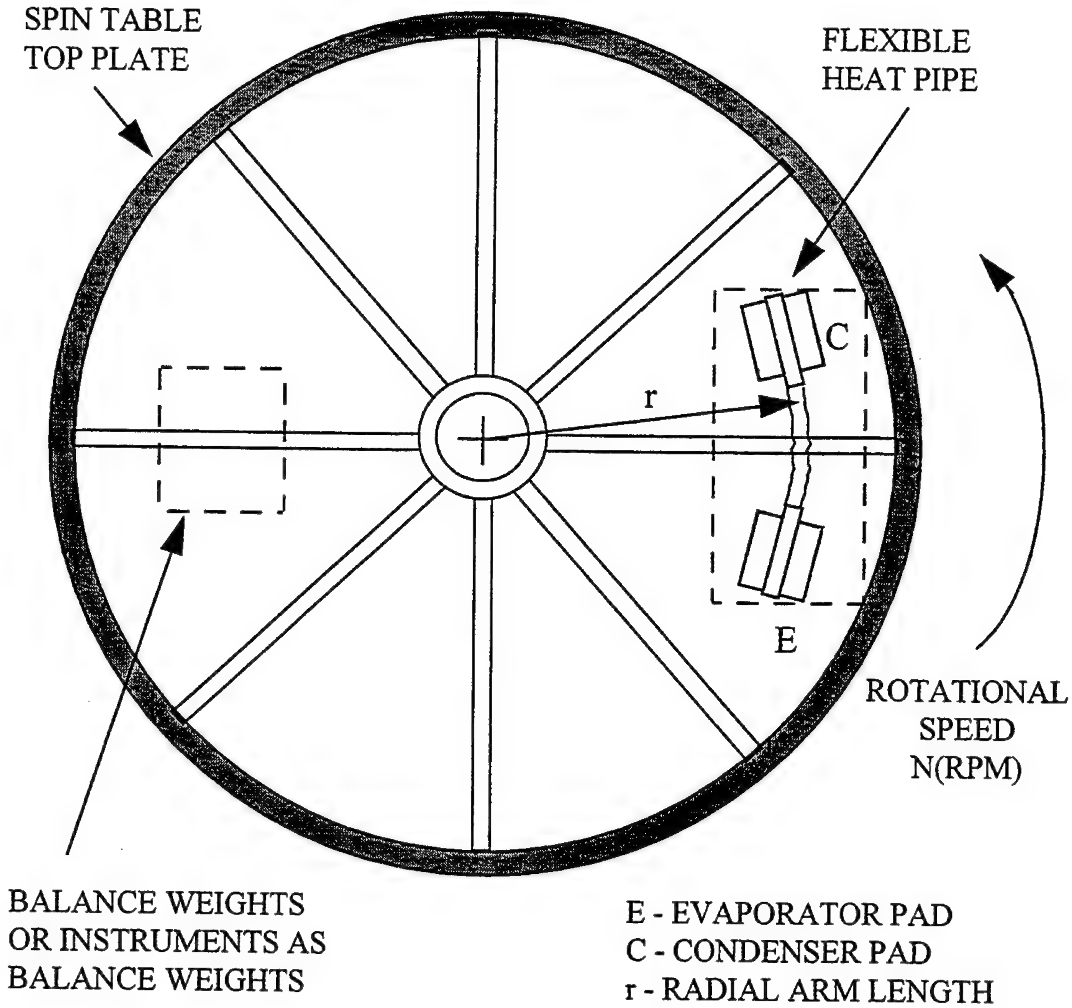

Figure 5. Top View of the Spin Table with Circumferentially Mounted Flexible Heat Pipe.

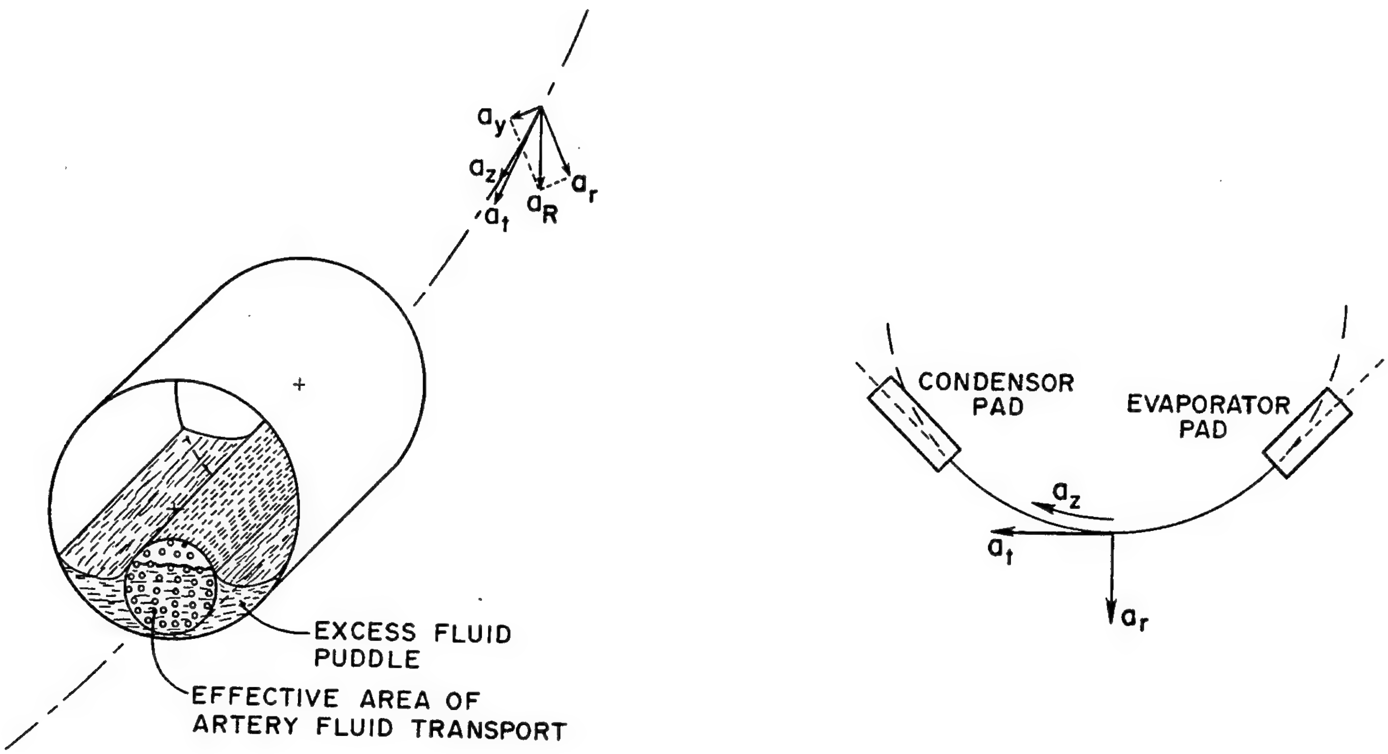

Figure 6. Acceleration Components Nomenclature.

2.2 EFFECT OF G-LOAD ON CAPILLARY LIMIT AND BOND NUMBER

The transport capability of a heat pipe is dependent on the maximum effective pumping pressure of the wick available at the evaporator. For steady-state operation of an arterial wick heat pipe in 1 G field and inclined at an angle ψ to the horizontal, transport capacity is as given in Eq. (3) obtained from Chi with usual notations.[1]

$$\int_0^L (F_\ell + F_v) Q dx = \frac{2\sigma}{r_c} + \rho_\ell g d \cos\psi + \rho_\ell g L \sin\psi \tag{3}$$

For a heat pipe in an accelerating environment, Eq. (3) has to be modified in order to account for the body forces generated by the resultant acceleration (a_R). The modified equation is

$$\int_0^L (F_\ell + F_v) Q\,dx = \frac{2\sigma}{r_c} + \rho_\ell a_R d \cos\psi + \rho_\ell a_R L \sin\psi + \int_0^L \rho_\ell a_t dx \qquad (4)$$

The last term on the right hand side of Eq. (4) is zero for the circumferential mounting steady-state conditions. Also, the term sin $\psi = 0$ for horizontal mounting. The pressure loss or gain due to the induced acceleration depends on the magnitude and direction of a_R which in turn depends on the mounting and rotation details. It may be noted here that essentially Eq. (4) simplifies to a situation similar to that of Eq. (3) where g is replaced with a_R. For a rigorous treatment of this study, Eq. (3) should be considered with components of the induced acceleration in all directions together with g.

Theoretical capillary transport limit for the flexible copper-water heat pipe (described in the Appendix) has been estimated using Eq. (4) for a_R = 1G, 4G and 10G and plotted along with experimental results. The effective capillary radius (r_c) of the artery cable wick was calculated based on the adverse tilt test results and using Eq. (5).

$$r_c = \frac{2\sigma\cos\theta}{\rho_\ell g H} \qquad (5)$$

The extrapolated wicking height (H) was 24.8 cm and the corresponding $r_c = 0.554\times10^{-4}$ m whereas the measured $r_c = 3.06\times10^{-4}$ m. Both, the low and high values, were used in calculations.

2.2.1 Transverse Load (Circumferential Mounting)

It is assumed that the flexible heat pipe was mounted horizontally on the spin table with its longitudinal axis along a circular arc at a radius of 1.0 m from the center of the table as shown in Figure 5. Under steady spin rate, the radial acceleration experienced by the fluid in the artery cable is uniform along its length. The ability of the artery cable to retain fluid can be determined by a pressure balance involving the surface tension force in the wick and the radial gravity (induced) force. The condition in Eq. (6) must be satisfied in order to keep the artery cable primed under radial acceleration. Vertical acceleration a_y is assumed to be zero, and hence, a_R=a_T.

$$\begin{Bmatrix} \text{Pressure exerted on the} \\ \text{fluid in the wick due} \\ \text{to radial gravity force} \end{Bmatrix} \leq \begin{Bmatrix} \text{Capillary pressure available} \\ \text{in the wick due to} \\ \text{surface tension} \end{Bmatrix} \tag{6}$$

For an artery cable wick of length L, diameter d, porosity ϵ and capillary pore radius r_c, and assuming uniform cross section and wick porosity, Eq. (6) can be written as

$$\frac{\pi d^2}{4} \frac{L\varepsilon(\rho_\ell - \rho_V)}{Ld} a_r \leq \frac{2\sigma\cos\theta}{r_c}$$

Simplifying,

$$\frac{a_r(\rho_\ell - \rho_v)dr_c}{\sigma} \leq \frac{8\cos\theta}{\pi\epsilon} \tag{7}$$

The left-hand side of Eq. (7) can be recognized as the Bond number for this case.

That is,
$$Bo_1 = \frac{a_r(\rho_\ell - \rho_v)dr_c}{\sigma}$$

For the wick under consideration, $\epsilon = 0.4125$ and assuming perfect wetting ($\theta = 0$), Eq. (7) becomes

$$Bo_1 \leq 6.173 \tag{8}$$

Bond number for the present wick-fluid system (copper-water), can be determined as a function of the heat pipe operating temperature at various radial G-loads. Figure 7 illustrates that the flexible heat pipe can be operated safely at 10 G in the circumferential mounting. As the Bond number cannot be experimentally determined, the regions of high-G tests performed on the present heat pipe for two cases of r_c values and a_r=10.1 G are marked in this figure. Uncertainties in determining the wick parameters (r_c,θ,ϵ) will directly affect the Bond number which will in turn influence the limit on radial G-load. In addition, liquid inventory, puddling

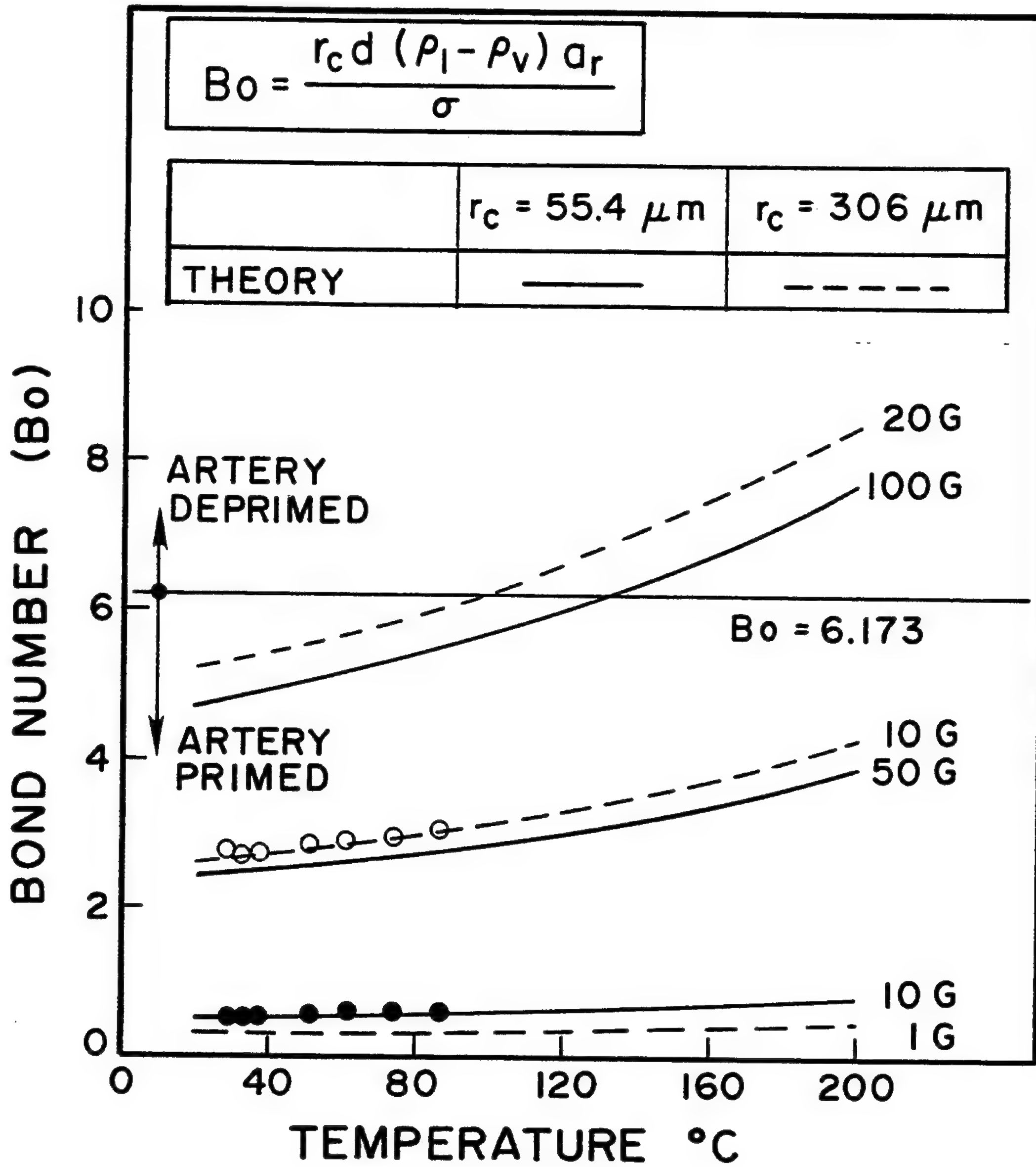

Figure 7. Effect of Radial Acceleration on Heat Pipe Performance for Circumferential Mounting (Bond Number vs Temperature).

Note: The open and closed circle data points on the graph indicate the maximum G-level of tests actually conducted without depriming the artery.

effects and arterial depriming due to partial saturation may all affect the transport limit under G-load.

2.2.2 Longitudinal Load (Radial Mounting)

The following assumptions and conditions are made for analyzing the radial mounting of the heat pipe on the spin table:

- Planar mounting on the spin table along a radial line (Figure 8)
- Steady-state of spin (ω = constant)
- Heat pipe has uniform cross section
- Wick porosity is uniform
- Evaporator end is nearer to the center of the spin table (unfavorable wicking condition)

The condition for the working fluid to prime the wick segment dx can be expressed as

$$\int_{x_1}^{x_2} \left(\rho_\ell - \rho_V\right) \epsilon \omega^2 x \, dx \le \frac{2\sigma\cos\theta}{r_c} \tag{9}$$

or

$$\left(\rho_\ell - \rho_V\right) \epsilon \omega^2 \frac{\left(x_2^2 - x_1^2\right)}{2} \le \frac{2\sigma\cos\theta}{r_c}$$

(10)

rearranging,

$$\frac{\left(\rho_\ell - \rho_V\right) \omega^2 \left(x_1 + \frac{L}{2}\right) L \, r_c}{\sigma} \le \frac{2\cos\theta}{\epsilon}$$

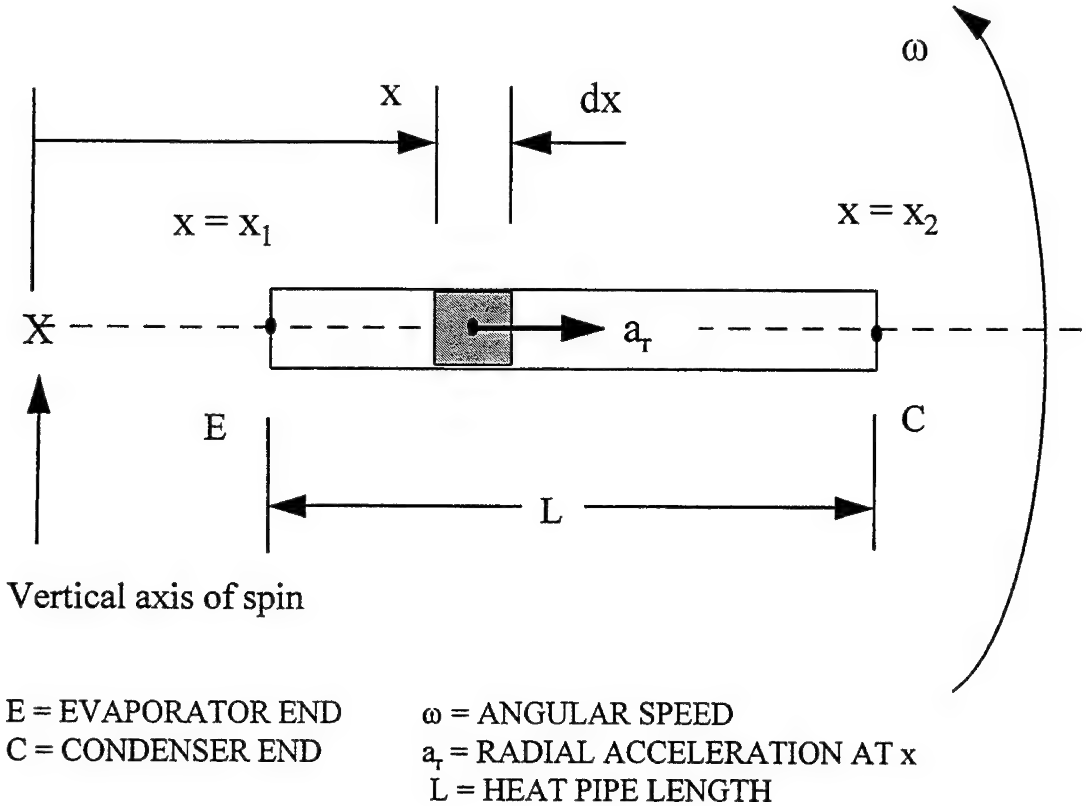

Figure 8. Radial Mounting of a Straight Pipe on the Spin Table.

A Bond number can be defined here using the average centrifugal acceleration (radial) term,

$$\bar{a}_r = \omega^2\left(x_1 + \frac{L}{2}\right) \text{ such that } \qquad Bo_2 = \frac{(\rho_\ell - \rho_v) L\, r_c\, \bar{a}_r}{\sigma} \tag{11}$$

For the wick under consideration, $\epsilon = 0.4125$ and for complete wetting ($\theta = 0$), above equation becomes

$$Bo_2 \leq 4.848 \tag{12}$$

Bond number (Bo_2) for the flexible heat pipe ($L = 0.762$ m) mounted radially on the spin table with $x_1 = 0.25$ m and $x_2 = 1.012$ m is calculated based on Eq. (11) as a function of the pipe operating temperature for three values of radial G's, $a_r = 0.8$ G, 1.0 G and 1.6 G. The results are plotted as shown in Figure 9 and it is clear that the heat pipe artery will be deprimed if the operating conditions exceed $a_r = 1$ G and 80°C. It should be noted here that the mounting orientation is the most unfavorable wicking condition which must be avoided in practical situations of steady radial acceleration conditions. However, transient radial acceleration loads may have a completely different priming or depriming behavior of the wick and that will require further study.

3.0 DESIGN AND DEVELOPMENT OF A SPIN TABLE TEST FACILITY

3.1 DESIGN REQUIREMENTS

Air Force anticipates a number of thermal management related problems in connection with the more-electric aircraft components development. These include auxiliary power units (APU), starter/generators, brakes, flight control surface actuators, etc. Heat pipe and phase change material (PCM) thermal control methods may be applied in these devices.

One immediate requirement which had to be addressed was to test the flexible heat pipe developed by the Navy and Thermacore under an SBIR program for cooling the actuator of an F/A-18. Before a new heat pipe device can be installed on an aircraft system, simulated ground

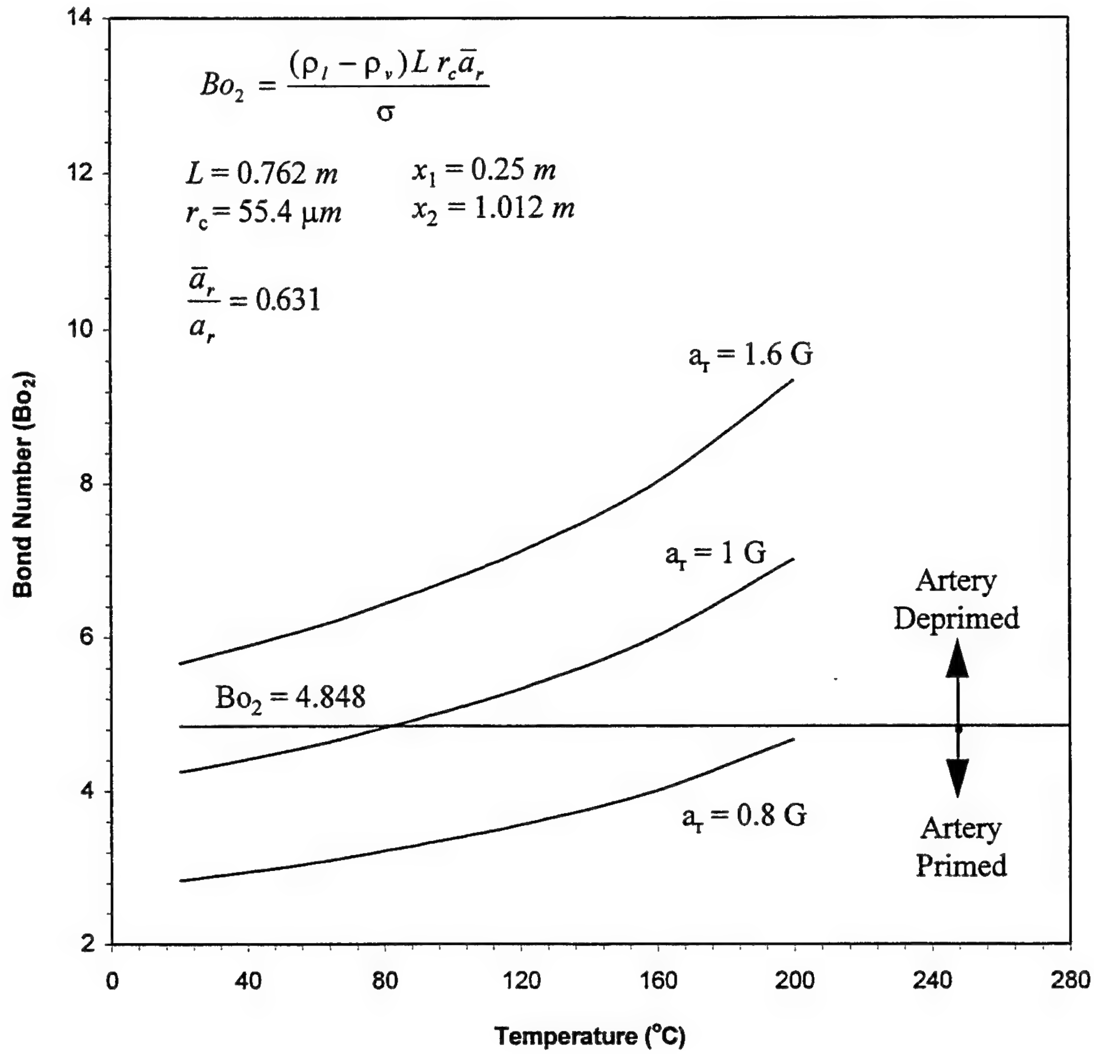

Figure 9. Effect of Centrifugal Acceleration on Heat Pipe Performance for Radial Mounting.

tests have to be performed. In this regard, a spin table test setup was necessary and the features/capabilities required were as follows:

•	Style:	Horizontal table with forward/reverse rotations; multichannel signal and power slip rings; coolant feed-through
•	G-load:	10 Gs maximum
•	Acceleration rate:	3 G/sec spin up 2 G/sec spin down
•	Test item weight:	50 lb.

An old surplus facility donated by the Air Force Aerospace Medicine Division was refurbished and instrumented for this purpose. Presently, this test facility is functional at the H-Bay Thermal Laboratory in Building B71.

3.2 SPIN TABLE TEST FACILITY DESCRIPTION

The setup consists of a 2.4 m diameter table mounted on a vertical shaft and thrust bearing assembly. A 20 HP dc motor drives the table through a reduction gear box with gear ratio 8.75:1. The table can be spun at any speed in the range 0-100 rpm. A triaxial accelerometer mounted on the table measures the accelerations in radial, tangential and vertical directions. Electrical power to heat pipe is fed through disc shaped rings and carbon brushes mounted at the bottom of the table. Instrumentation signals from thermocouples and accelerometers are taken out through an instrumentation quality 40-channel slip ring assembly mounted on the vertical shaft above the table. A four-port hydraulic rotary coupler services the coolant to the heat pipe. A constant temperature bath circulates 50/50 by mass ethylene glycol-water mixture through a flowmeter to the heat pipe condenser. Thermocouple signal conditions are kept on the spin table itself in order to reduce electrical noise in transmission and slip ring motion. Counterbalance weights are used on the table to minimize dynamic imbalance of the table. The heat pipe is insulated thoroughly to ensure accurate calorimetric measurements. Figure 10 shows the major components of the spin table and overall dimension and weight details.

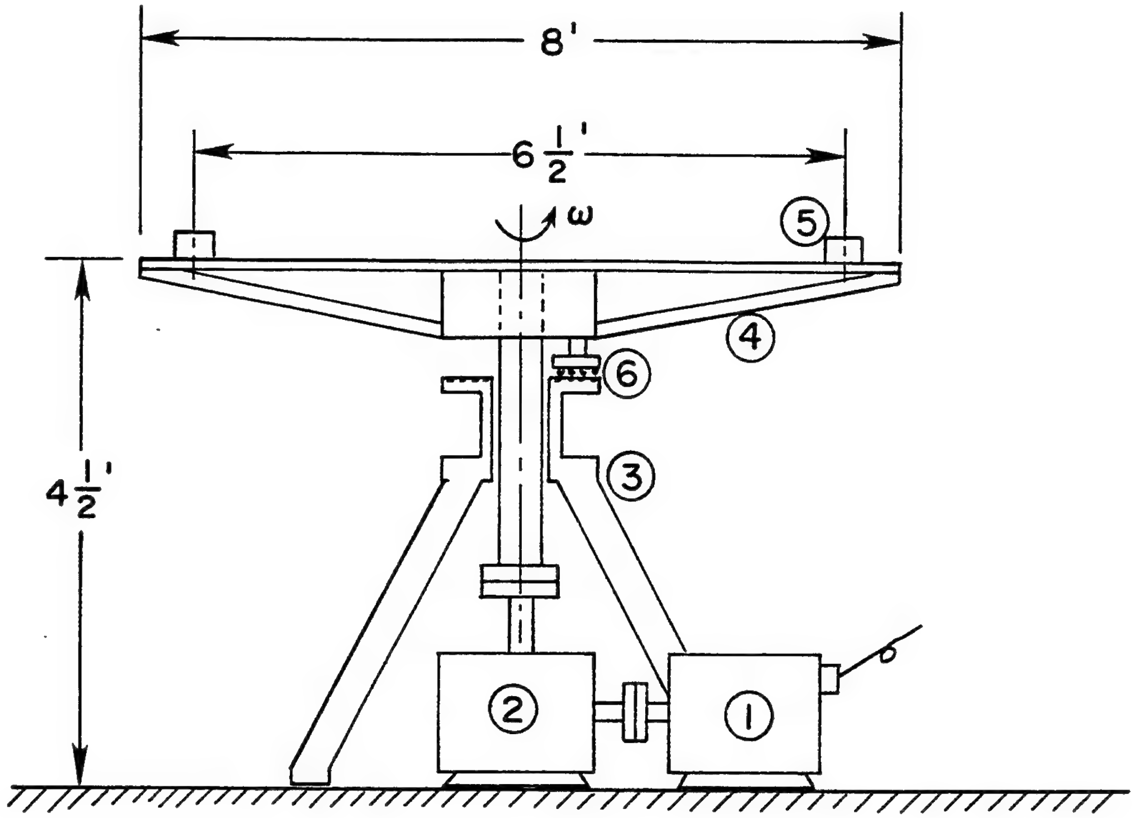

① Motor	<u>Weight</u>		
② Gear Box (8.75 : 1)	Table	330 lb.	
③ Stand	Hub, Shaft, Bearing	190 lb.	
④ Table	Test Item	50 lb.	
⑤ Test Specimen	<u>Speed Control</u>		
⑥ Slip Ring Disc/Brush Pickup	Vary Table Speed	0 - 100 (RPM)	

Figure 10. Spin Table Major Components.

3.2.1 Drive System

The following are the motor drive and control specifications:

Motor: 20 HP, 1150 RPM base DC shunt wound motor

- 240V armature
- Frame 2812AT
- Blower and filter
- 240V field STD
- Drip-proof guarded
- GE Kinematic motor

Motor Control: CMC PM12 Regen package:

- 4 quad system
- AC line inductors - SP1-101
- Regen to stop
- AC line circuit breaker
- Speed and load meters
- Fused blower motor starter
- NEMA 12 enclosure
- Interlocked thru the door circuit breaker
- Remote enclosure NEMA 13
- Armature voltage feedback 2%
- AC input 22 amps @ 460/3/60
- Arm, DC amps 75 @ 240V
- Field amps 5 max @ 240V
- "A" module PM12-A-020AP
- NEMA 12 ventilated enclosure - 42"H×30"W×12"D
- Wall mounted
- Armature inductor for using old motor

Operator control station for remote location NEMA 12, start/stop speed pot, "power on" light, "run" light, isolation transformer 460V/3 ph/60 Hz primary, 1-57 tap above or below spec., 230V/3 ph/60 Hz secondary.

3.2.2 Slip Ring Assembly

The spin table has two slip ring assemblies. One is disc shaped rings with sturdy carbon brushes for power feeding up to 5 amp load. Six such concentric rings and pickups are mounted on the bottom of the table. The other slip ring is a 42 channel instrumentation type system with through mounting over a shaft. This consists of a cylindrical grooved type ring and two brush blocks with 21 channels each, located outside the cylinder. Each channel has two contactors. Figure 11 shows the details of this slip ring along with a rotary hydraulic coupling.

3.2.3 Data Acquisition System

A summary of the details of the instrumentation and data acquisition system is given below.

- Keithley 575 with AIM2 card and data bus to work over 150 ft; RS-422 port compatible.

- PC with RS-422 or IEEE port
  VGA graphics, hard disk 40 MB, 1 MB RAM

- Menu-driven software
  Real time
  Foreground/background application, multiplexing
  Control D/A outputs
  Quick Basic programming
  500-1000 Hz scan rate

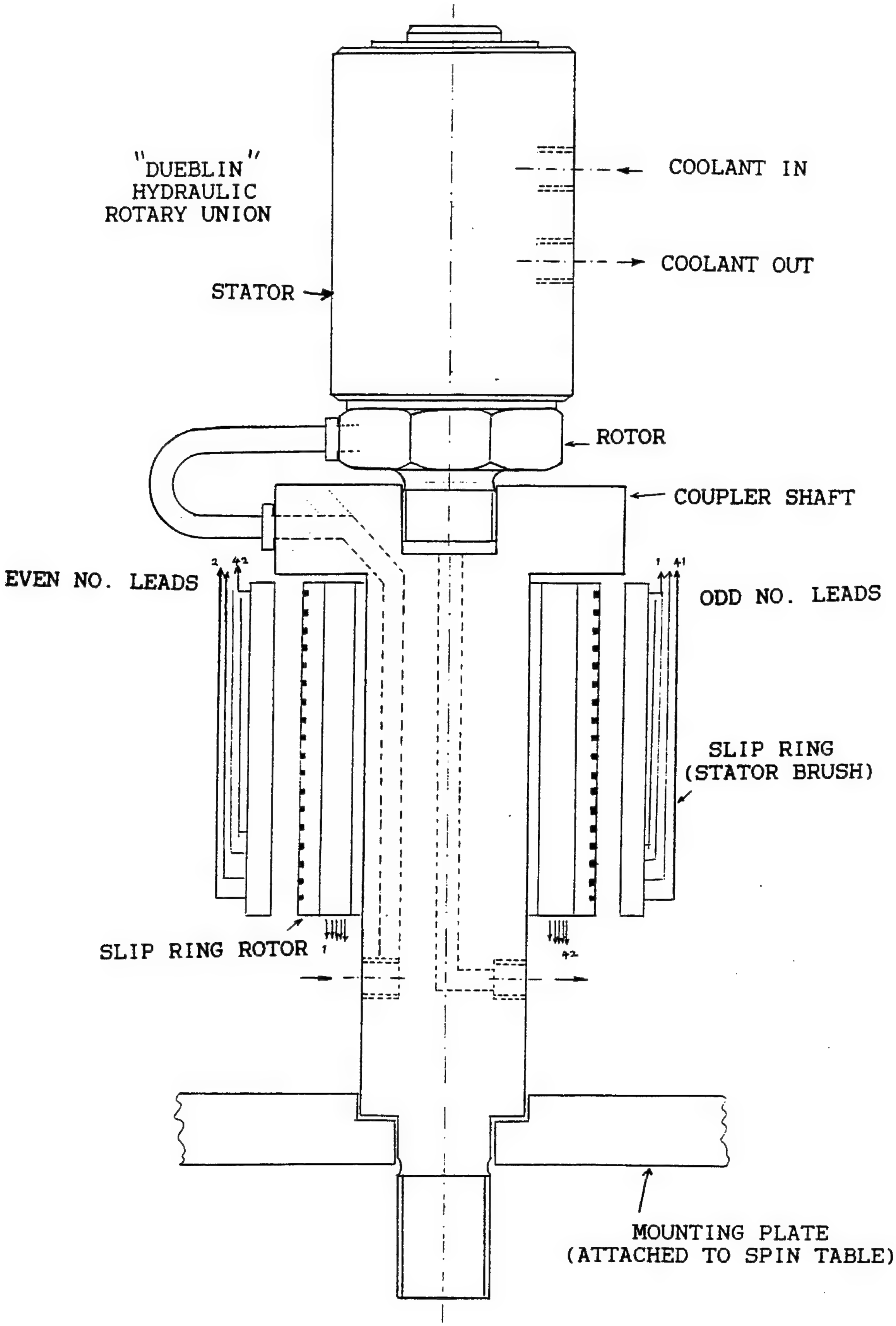

Figure 11. Slip Ring and Rotary Hydraulic Union Assembly for the Centrifuge Table.

- Input

  16 thermocouples through signal conditioners 0-5 VDC

  3 accelerometer (triaxial) channels ±7.5 VDC

  1 tachometer 0-5 VDC

  1 flowmeter 0-5 VDC

  2 AC voltage through signal conditioners 0-10 VDC

- Output

  1 D/A signal for motor control 0-10 VDC, 4-20 mA

- Signal Conditioners

  16 self-linearizing thermocouple input modules ±0.5 °C accuracy; mother board for signal conditioners

- Sensors

  Thermocouples (K-types), three axis accelerometer (0-15G), flowmeter (0-2 gpm)

A schematic diagram of the integrated spin table with all the controls and instrumentation systems is shown in Figure 12. For safety reasons, the spin table and the control station are separated. A closed circuit television camera and monitor system is used for visual observation and control.

4.0 EXPERIMENTAL WORK

4.1 HEAT PIPE TEST HARDWARE

The candidate test heat pipe used in this effort was designed and fabricated by Thermacore, Inc. This pipe was one of the four flexible heat pipe cold plates (FHPCP) built to provide cooling for either the electronic package mounted on an aileron actuator or a remote terminal electronics package for a trailing edge flap actuator aboard the Navy F/A-18. A detailed

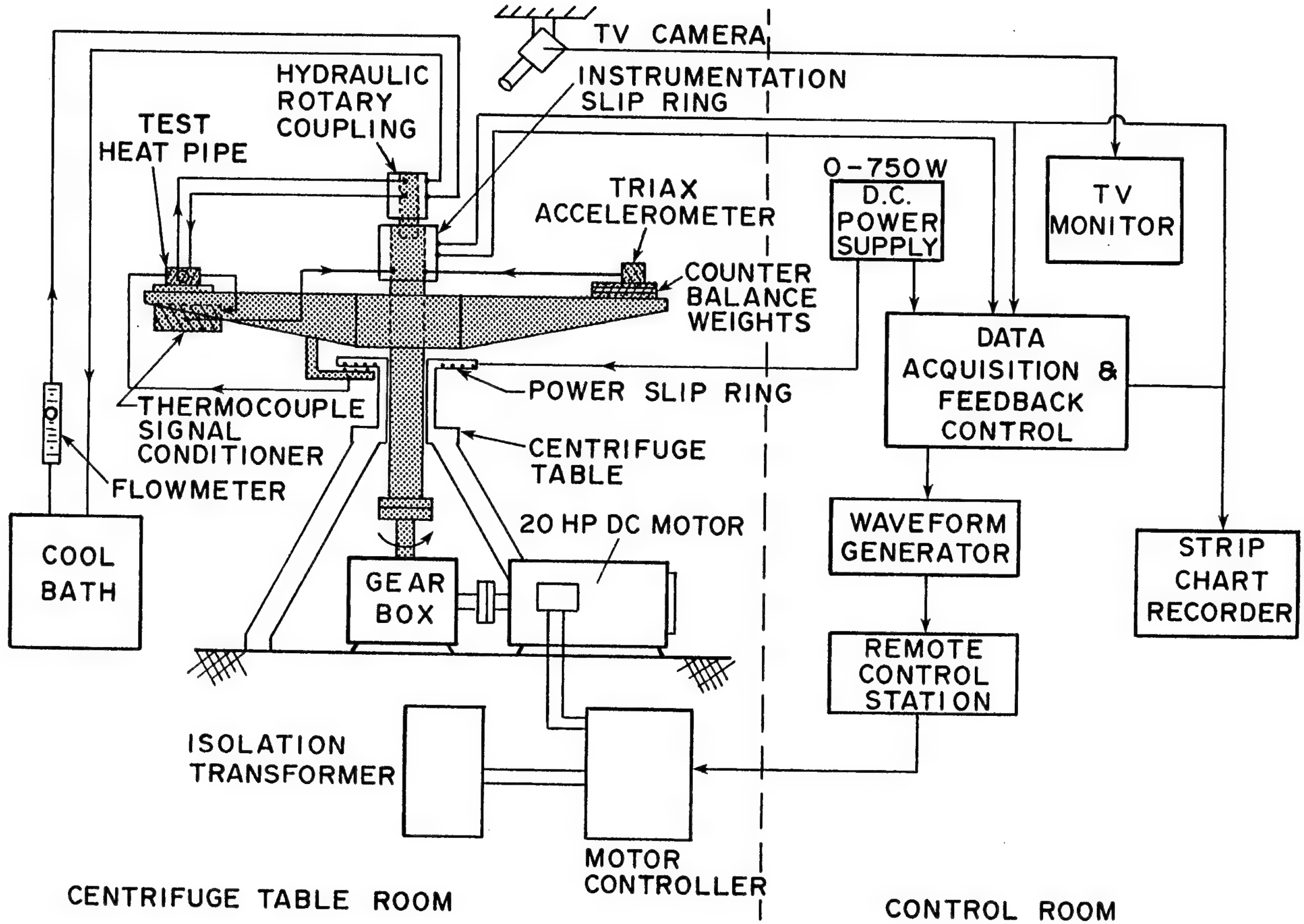

Figure 12. Schematic Diagram of the Integrated Spin Table.

description of the design and fabrication aspects can be found in Ref. 2 and the static transient thermal performance results for step changes in heat input can be obtained from Ref. 11. Additional data on transient heat flux effects and body force effects can be seen in Ref. 12. Table 2 provides the summary of design details for this heat pipe.

A perspective view of the flexible heat pipe showing the evaporator and condenser pads and a cut away view of the artery cable in the adiabatic section is illustrated in Figure 13. The physical dimensions and the thermocouple locations are provided in Figure 14. The condenser pad was cooled by a water-ethylene glycol mixture circulated cold shoe. A constant temperature bath and calibrated rotameter aided calorimetric measurements. The evaporator was heated by MINCO foil heater which was fed by a controllable power supply. Photographic views of the heat pipe mounted on the spin table in circumferential orientation are given in Figures 15(a) and (b).

4.2 STEADY-STATE PERFORMANCE TEST PROCEDURE

Steady-state performance tests were done on the heat pipe at various G-loads (transverse to the heat pipe axis) by maintaining the appropriate rotational speed for the table. The resultant acceleration a_R was obtained as $a_R = \sqrt{a_r^2 + a_y^2}$ where $a_y = 1G$ due to gravitational acceleration. Performance tests corresponding to static conditions were done at very low speed (≈ 10 rpm) in order not to damage the slip ring contacts. Typically at each G-load, heat input to the evaporator (Q_{in}) was raised in steps of 25 W initially and then in 5 W steps when evaporator dryout was approached. At each power setting, the temperature profile stabilized within 15-20 minutes. Test data included outputs from 15 thermocouples, triaxial accelerometer, power input and coolant flow rate. Data were scanned every minute and stored in disc files for subsequent processing. Heat actually transported through the heat pipe was obtained by calorimetric measurements. By steady state experimental measurements, it was determined that the transported power, Q_o, was 83.4% of the input power, Q_{in}. In all test runs, the condenser end was in the leading position. Table spin direction was not a contributing factor for steady state spin tests.

Reference 13 summarizes the steady state performance test procedure and test results.

Table 2. Design Details of the Flexible Heat Pipe

GENERAL	
Heat Pipe Length	73.7 cm
Design Power	59 Watts
Adverse Elevation at Design Power	7.6 cm
ΔT at Design Power	2.6°C
Working Fluid	Water
Working Fluid Charge	25 cc
Wall/Wick Materials	Copper
Total Weight	0.95 kg
EVAPORATOR	
Cold Plate Section	10.2 cm × 12.7 cm × 0.48 cm Copper
Envelope	OFHC Waveguide Tubing
Capillary Wick Material	+200/-325 Sintered Copper (1.01 mm thick)
POWDER (SINTER)	
Pore Radius	15.9 mm (expected); 55.4 μm (measured)*
Permeability	1.47×10^{-8} cm^2
FLEXIBLE ARTERY CABLE	
Type	Braided Cable
Vendor	New England Electric Wire Co.
Construction	24×7×36 over 7×37/30
Material	OFHC Copper
Pore Radius	306 μm
Permeability	5.77×10^{-6} cm^2
BELLOWS	
Length	45.7 cm (162 corrugations)
Diameter	1.3 cm i.d.
Vendor	Hydroflex Corp.
Part Number	HFAN-06-18-601-601-B1-CP
Rated Pressure	3.62×10^3 kPa
CONDENSER	
Wick Material	Spiral Grooves
Groove Pitch	60 grooves per 2.54 cm
Groove Depth	0.051 cm
Groove Angle	30° included
Tube Material	OFHC Copper
Tube Diameter	1.59 cm
Tube Wall Thickness	0.102 cm
Mounting Plate	3.2 cm × 1.52 cm × 0.48 cm

*Based on Thermacore's wicking height measurement of 9.75 in.

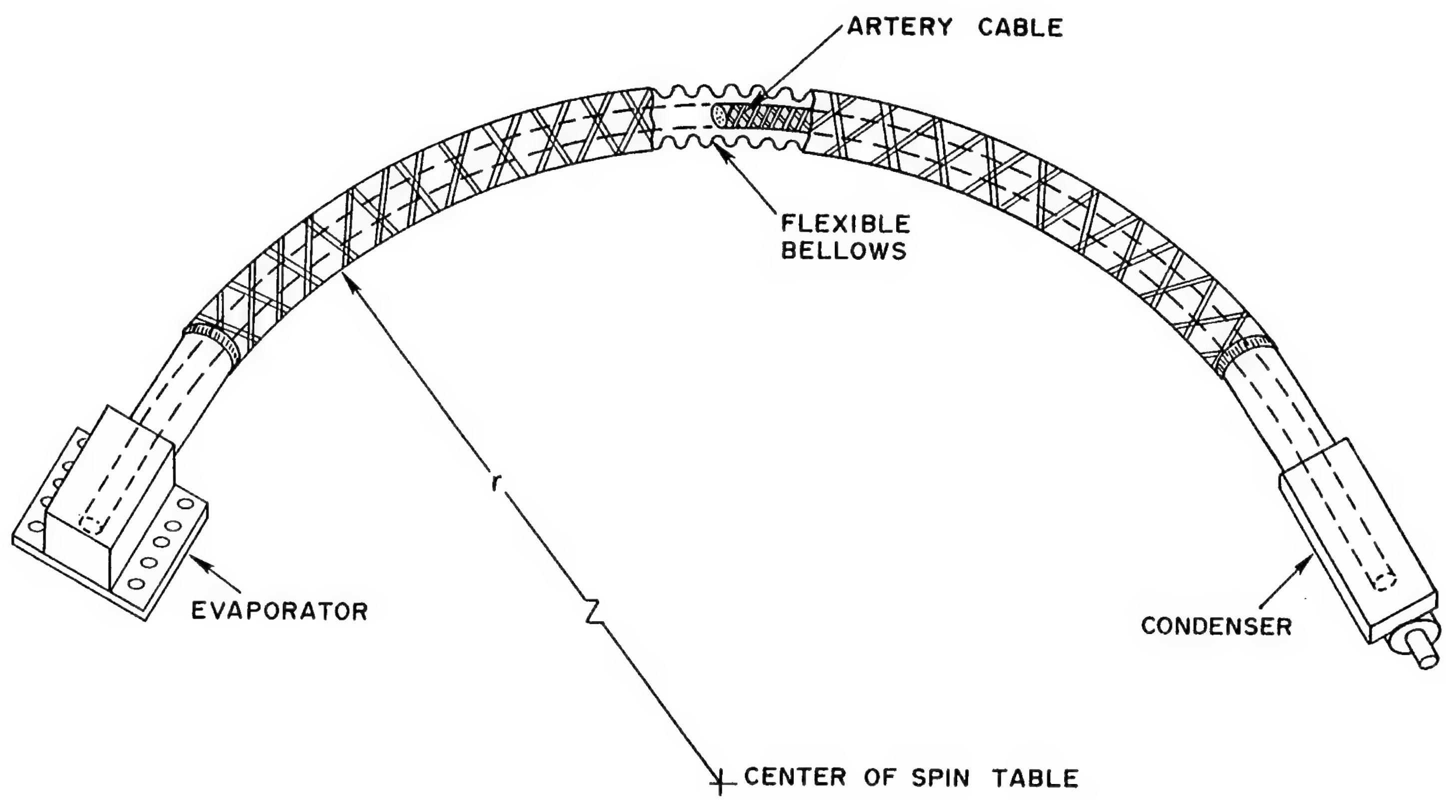

Figure 13. A Perspective View of the Flexible Heat Pipe.

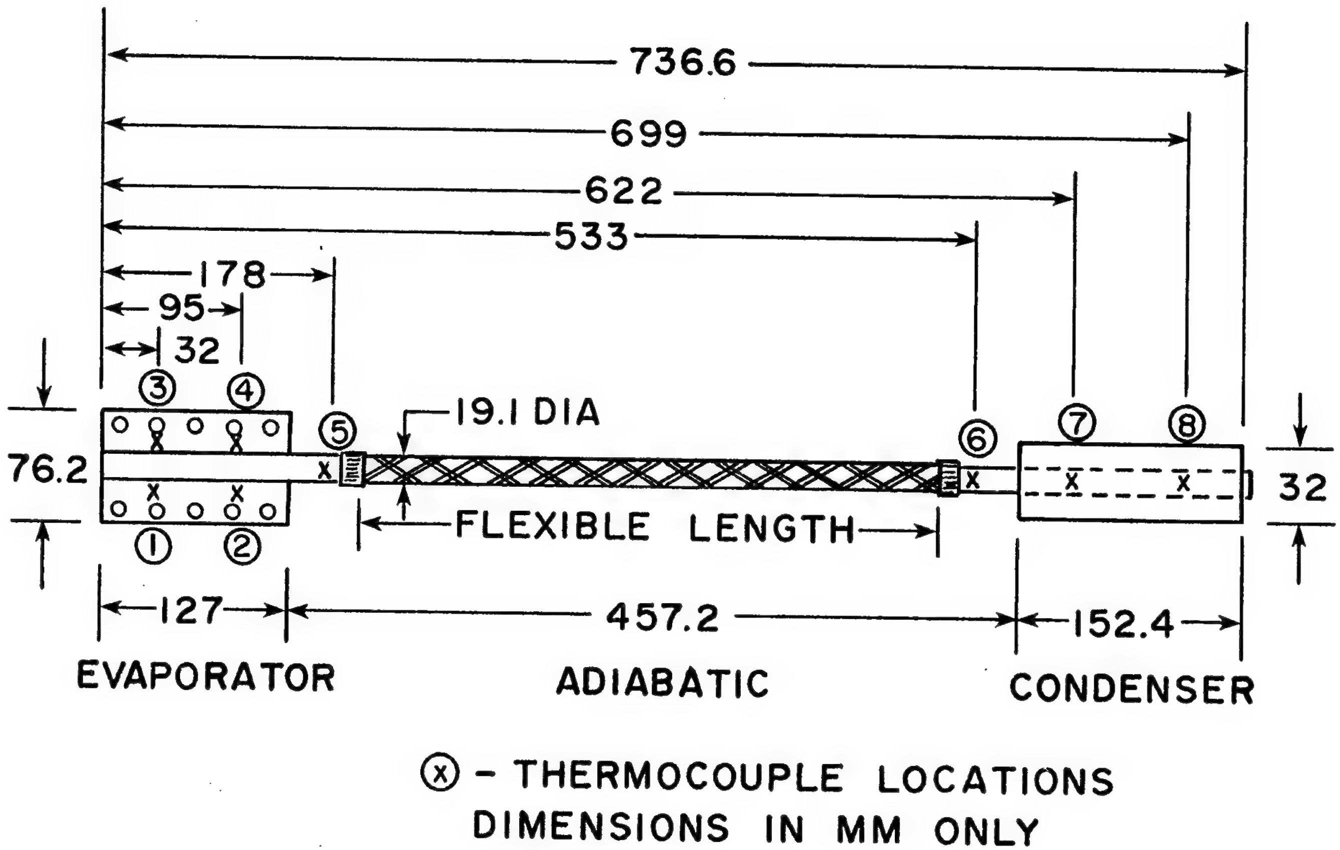

Figure 14. Physical Dimensions and Thermocouple Locations.

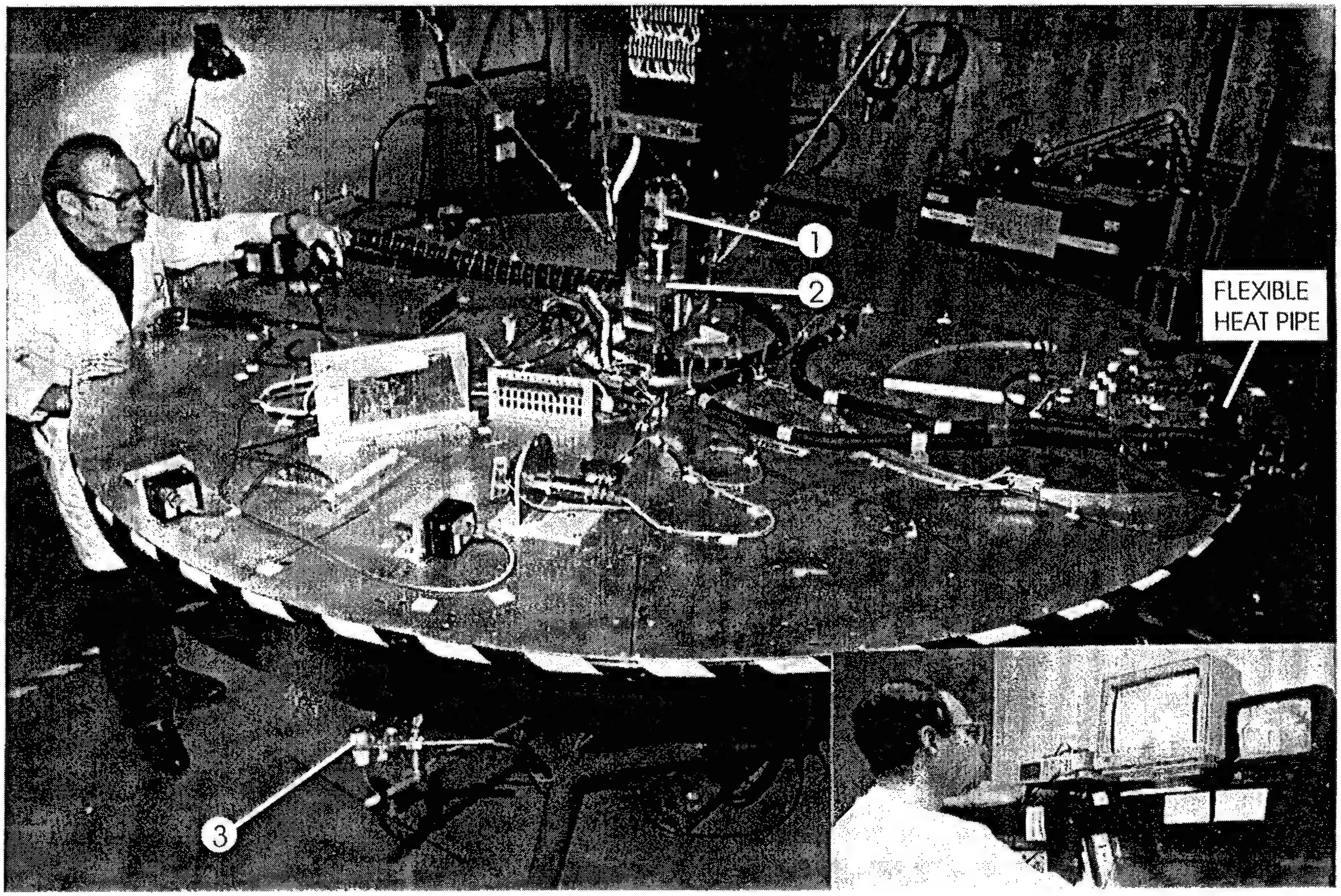

① Hydraulic Rotary Joint
② Slip Ring Assembly
③ Speed Sensor

Figure 15(a). Top View of the Spin Table with Circumferentially Mounted Flexible Heat Pipe (Inset: Controls Room).

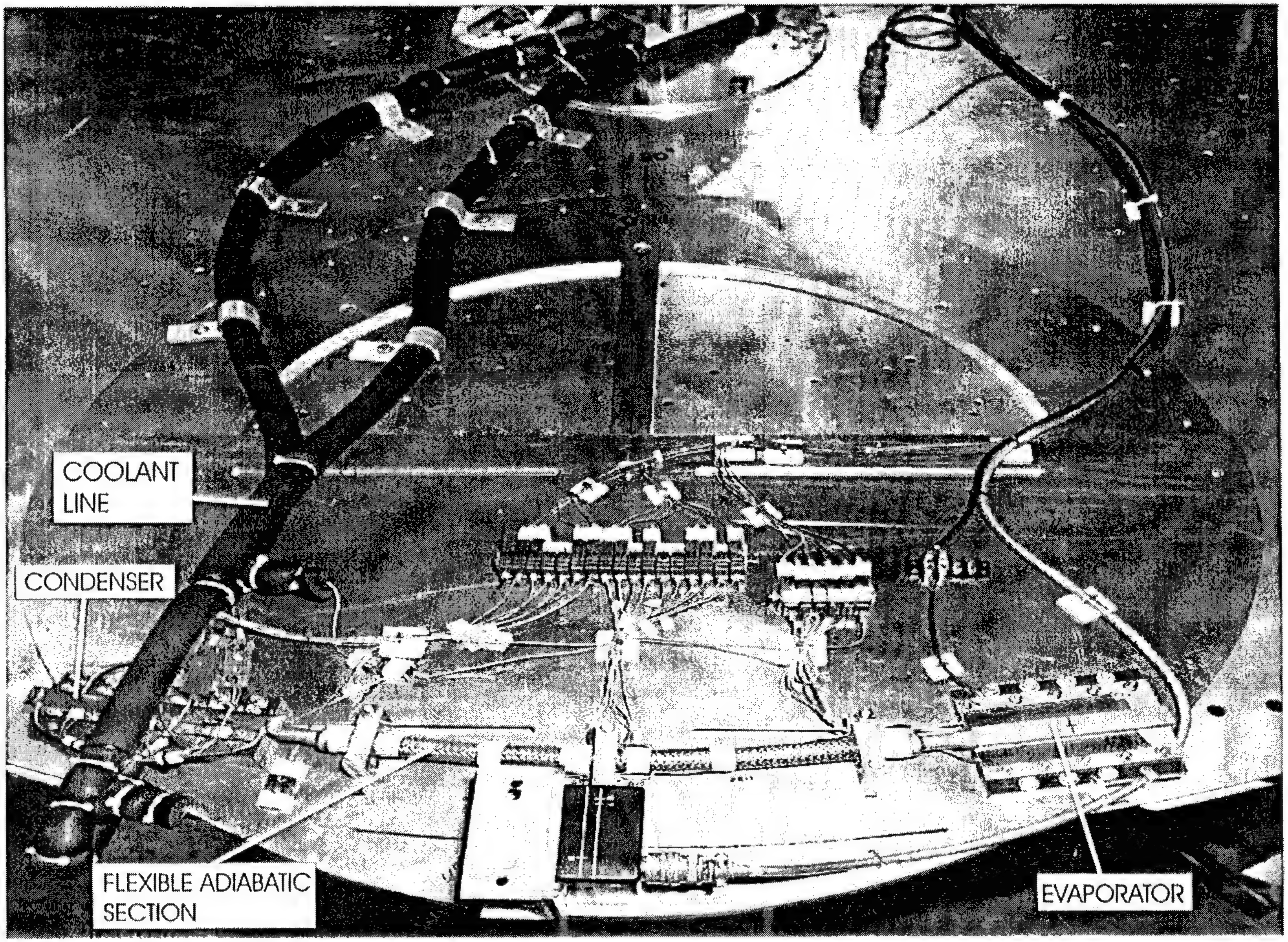

Figure 15(b). Close-up View of the Flexible Heat Pipe (Foam Insulation Removed).

5.0 RESULTS AND DISCUSSION

5.1 PERFORMANCE SUMMARY

The temperature profiles of evaporator pad, adiabatic section and condenser pad were plotted at each incremental power input level during the entire test duration ranging from 3-4 hours each. Figures 16, 17, 18 and 19 show these results for a_R = 1.01, 2.35, 4.35 and 10.10 G, respectively. A sudden rise in temperature of the evaporator pad at a threshold power level is distinctively noticeable in each of these cases. This point (where the evaporator end temperature exceeds that of the evaporator near the adiabatic section) marks a partial dryout of the evaporator wick and cautions against further increase of power input. It is also clear that this threshold power level progressively decreased with increase in G-load. Another important observation from these graphs is that at Q_o = 63 W, the evaporator operated at 36 ± 1%°C for all G-loads whereas the condenser temperature decreased with increase in G-load. The average temperatures of the heat pipe also decreased with increase in G-load. This is happening due to reduction in input power necessary for operating the pipe without evaporator dryout. These graphs clearly establish the safe operating limits for various G-loads. The cool down portions of those graphs are more or less the reverse of the heating mode. The repriming point of the evaporator wick and a slight hysterisis effect are clear.

5.2 AXIAL TEMPERATURE PROFILE

In order to illustrate the temperature profile along the length of the heat pipe, the test data at the near-dryout points (where the evaporator pad temperatures cross-over) from Figures 16-19 are retrieved and plotted as shown in Figure 20. The pipe operated with lower overall ΔT at 1.01 and 10.11 G than at intermediate G-loads. The adiabatic operating temperature dropped as a consequence of the drop in transported power which was triggered by increase in G.

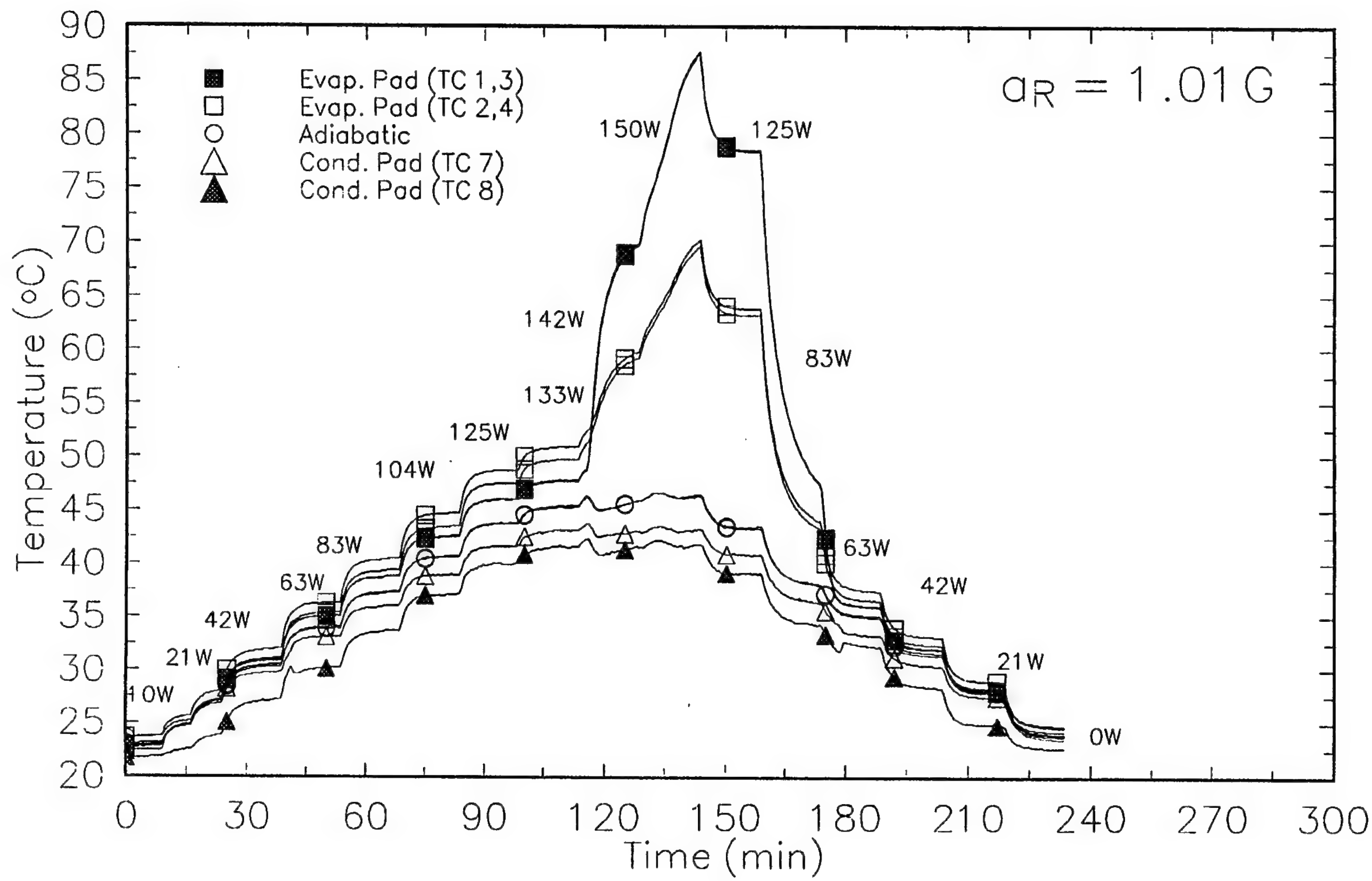

Figure 16. Steady-State Temperature Profiles for Various Power Increments at $a_R = 1.01$ G.

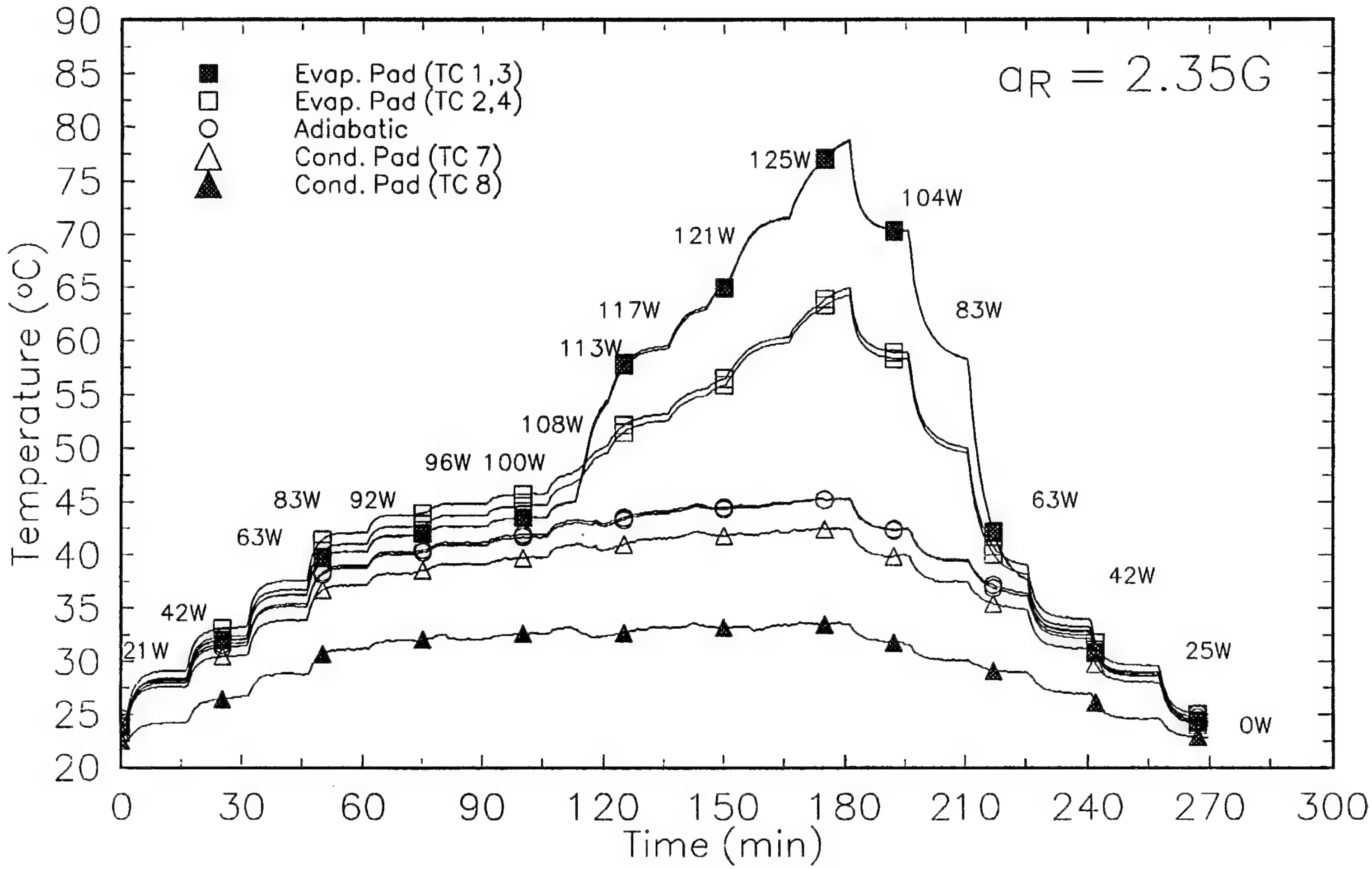

Figure 17. Steady-State Temperature Profiles for Various Power Increments at $a_R = 2.35$ G.

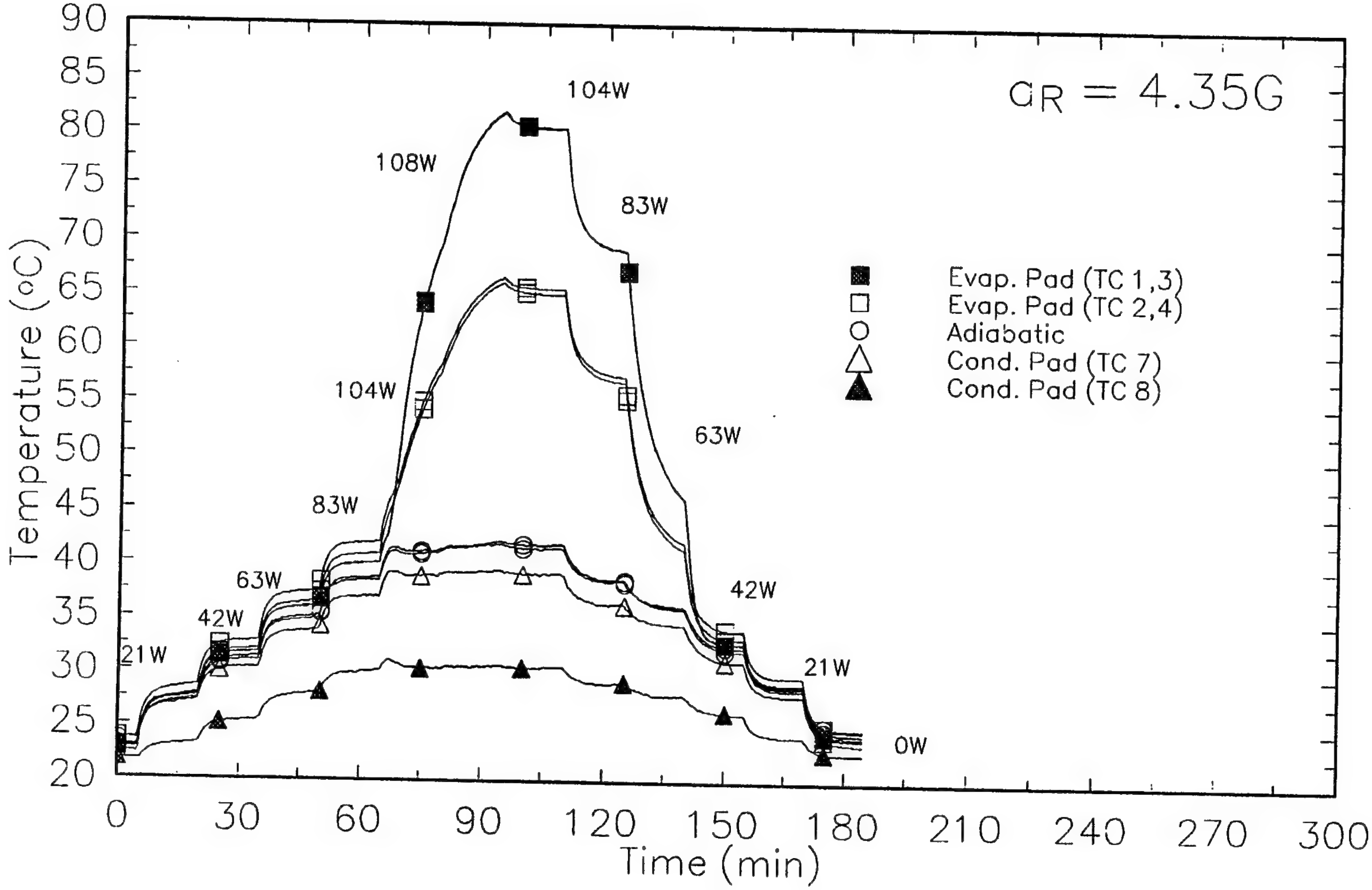

Figure 18. Steady-State Temperature Profiles for Various Power Increments at $a_R = 4.35$ G.

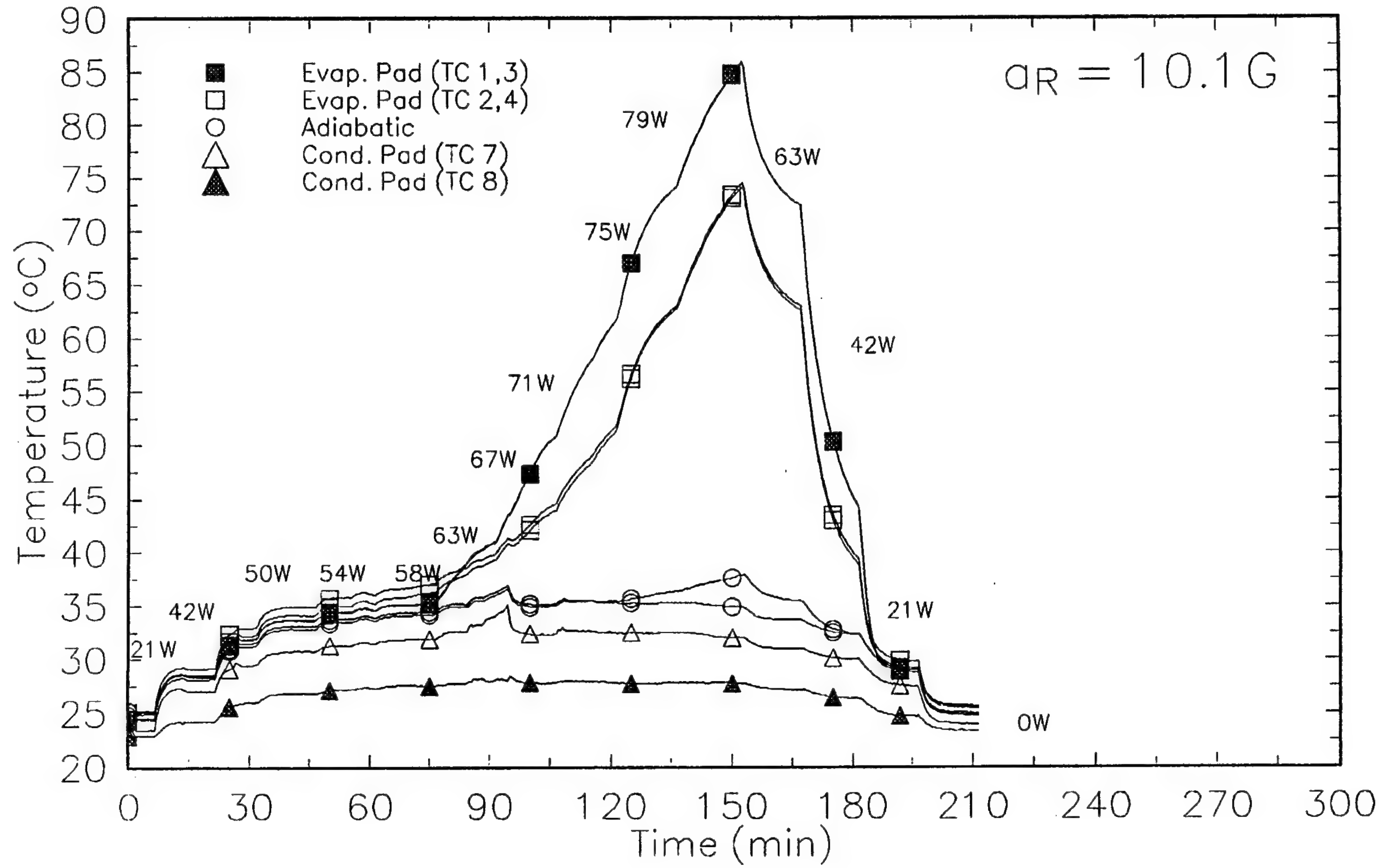

Figure 19. Steady-State Temperature Profiles for Various Power Increments at $a_R = 10.10$ G.

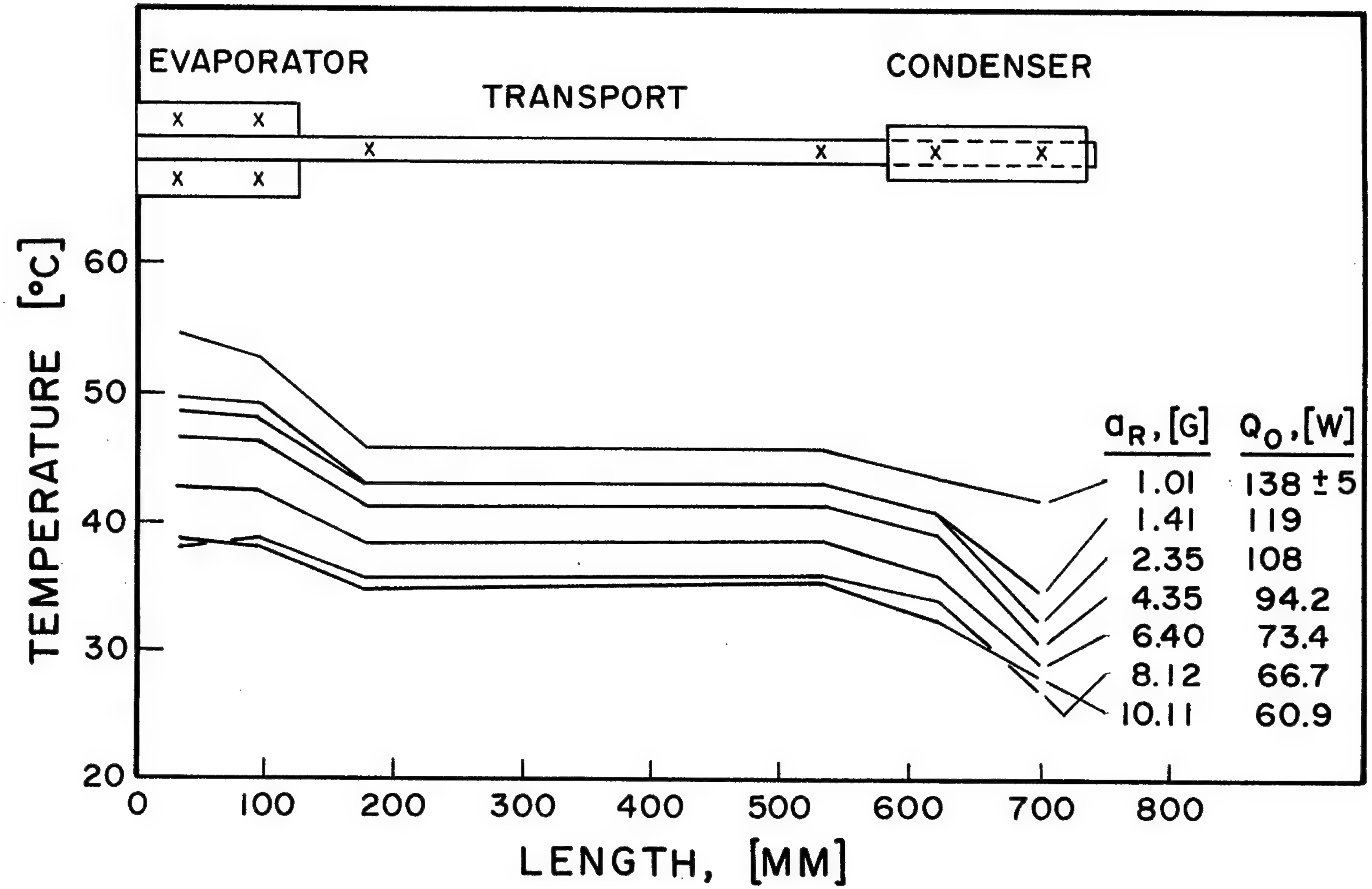

Figure 20. Axial Temperature Profile for Various Transverse G-Loads.

5.3 HEAT TRANSPORT RATE VS. TEMPERATURE DIFFERENCE

The transported power and temperature differences along the length of heat pipe are plotted as a function of transverse acceleration in Figure 21. Transported power dropped to lower than 50% of static performance. The design capacity of 60 W is still transportable at 10 G transverse. The temperature profile smoothing effect due to increase in G is apparent from the ΔT plots in Figure 21. Evaporator to adiabatic drop (ΔT_{EA}) steadily declined while adiabatic to condenser drop (ΔT_{AC}) increased at first and then dropped. The net effect is that the overall pipe ΔT decreased with G. The condenser efficiency is adversely affected at intermediate G loads due to puddling. Puddling of the condenser with excess fluid (and also the fluid forced out of the artery wick) occurs in the present mounting arrangement of the flexible heat pipe on the spin table. The straight sections of the evaporator and condenser pads stay off the circular mounting track and cause higher radial G at the ends. Temporary plugging of the condenser end shows high ΔT_{EA} up to 3 G. Further increase in G (3-10 G) forces the excess fluid to recede into the convolutions of the bellows thereby relieves the fluid plugging of the condenser and reduces ΔT_{AC}.

Various experimental operating points are plotted to show the heat transport capacity as a function of temperature in Figure 22. A theoretical capillary limit curve based on static condition pumping limit ($r_c = 0.5544\times10^{-4}$ m) is also shown for comparison. It appears that actual performance is better than that of theoretical at G-levels lower than 4.35. But at G-levels higher than 4.35 the actual performance is worse than the theoretical values. This anamoly may be due to the omission of g (gravitational acceleration) in calculating a_R in Eq. (4). The correct expression for a_R should be $a_R = \sqrt{a_r^2 + g^2}$. Due to uncertainties in determining physical parameters such as θ, ϵ, r_c and K, theoretical prediction of heat transport capacity may not be precise. Moreover, the validity of these wick parameters for high-G situations is unknown.

6.0 CONCLUSIONS

A comprehensive spin table test facility has been developed for testing heat pipes and other heat transfer experiments under high G loads.

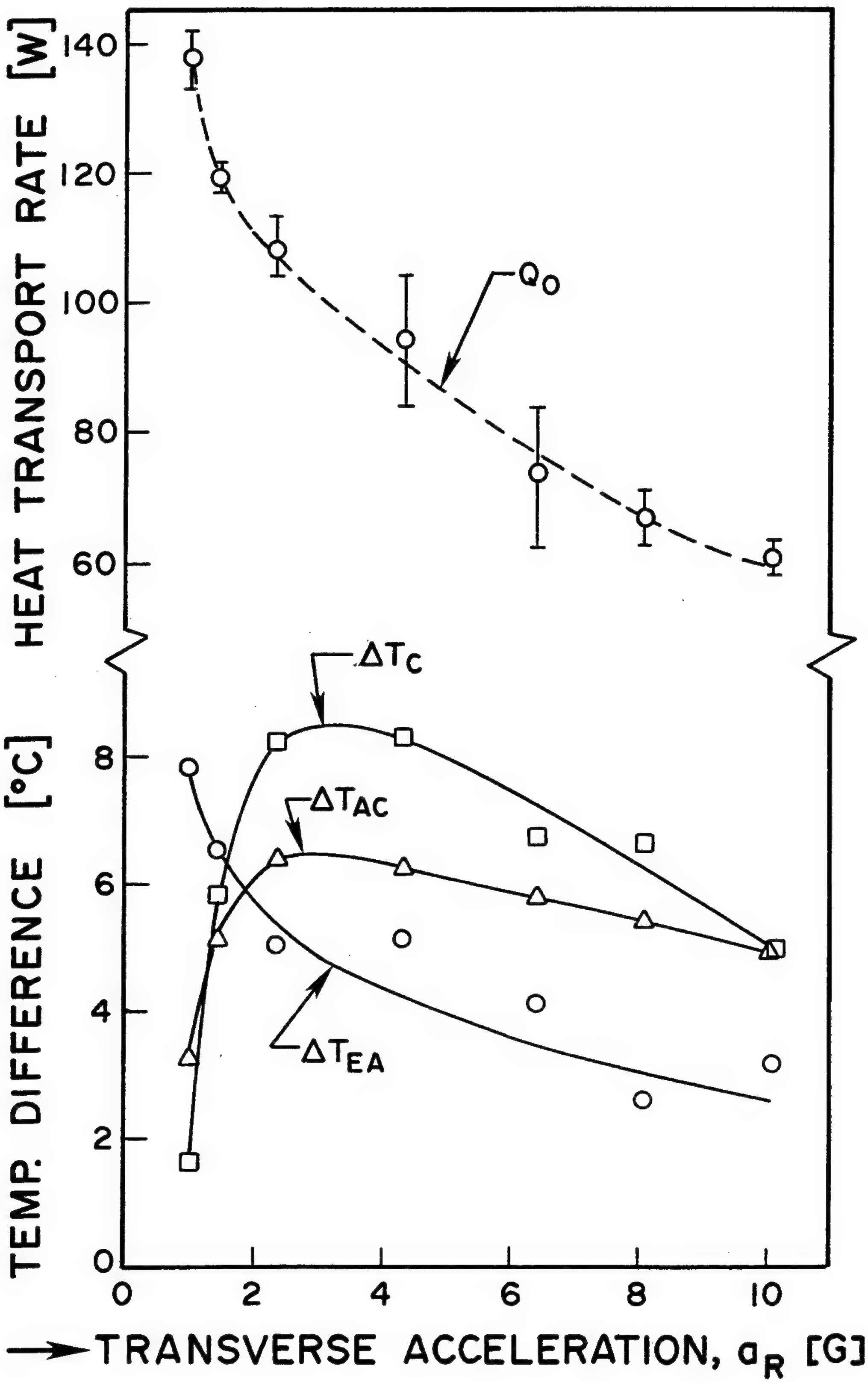

Figure 21. Heat Transport and Temperature Differences as a Function of Acceleration a_R.

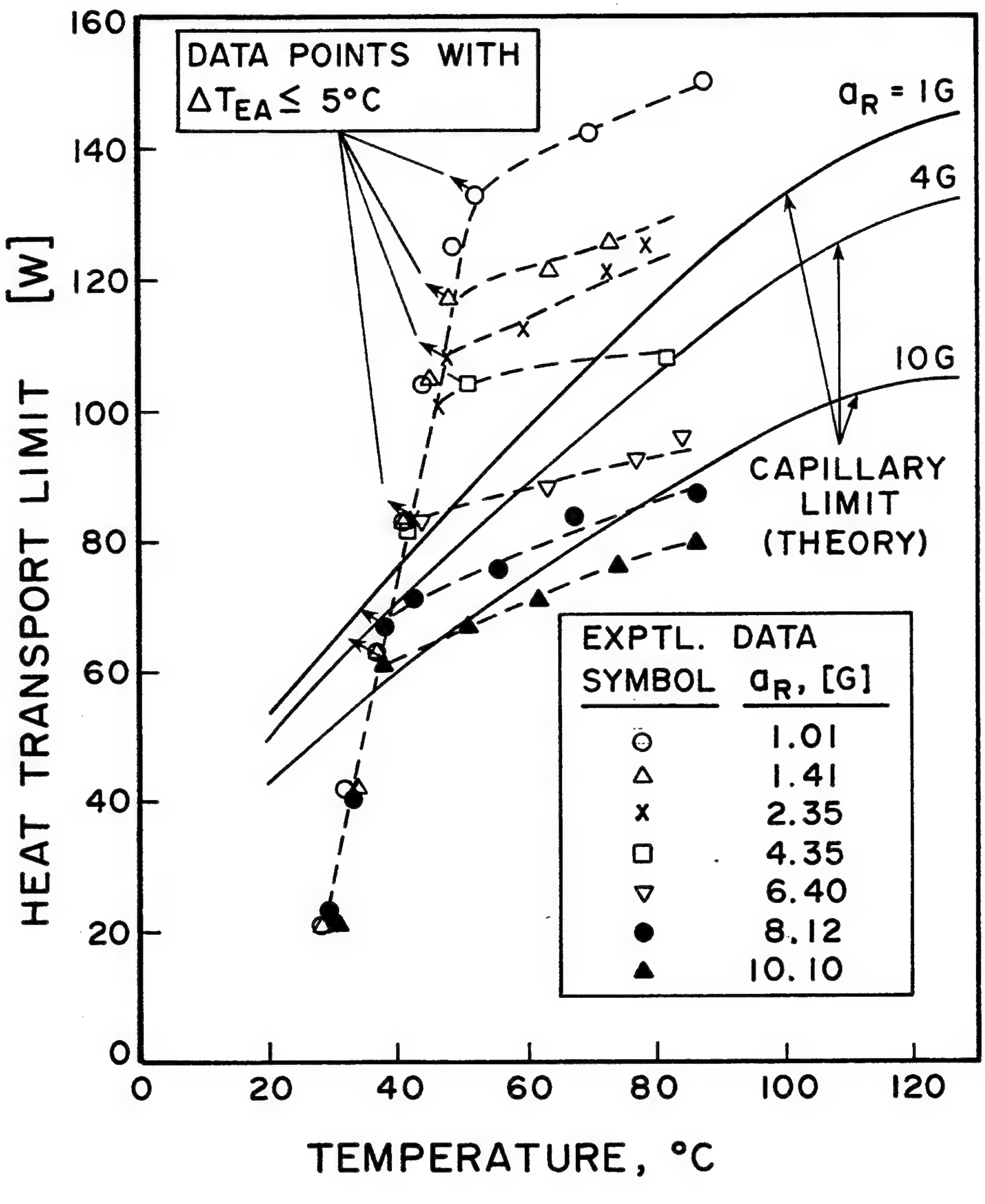

Figure 22. Effect of a_R on Heat Transport Limit.

A flexible copper-water heat pipe was instrumented and successfully performance tested on this spin table up to 98.1 m/s^2 acceleration load in the transverse direction to the heat pipe axis under steady-state conditions. The circumferential mounting orientation was based on the flight test acceleration loadings of the aircraft. Transport capacity dropped from 138 W for near-static condition to 60 W for 10 G condition. Overall temperature difference of the pipe at safe operating power range was more or less constant ($\approx 11\,°C$) up to 4 G and decreased to $8\,°C$ for 4-10 G. The decrease in ΔT at high G loads is due to even-distribution of fluid along the length of the wick. The bond number limit set for artery priming was not exceeded even at 10 G and assuming conservative capillary radius for the wick. Tests were not conducted with radial mounting orientation of the heat pipe for obvious reasons this orientation would simulate which are drastically favorable or unfavorable priming conditions. However, in the interest of verifying the analytical estimates, these tests may be performed.

This spin table and the instrumentation system are fully operational and form a versatile test facility for simulating G-loads of the military aircraft. It is expected that this facility would be utilized for a variety of heat transfer and thermal management research studies in the future.

7.0 REFERENCES

1. Chi, S.W., Heat Pipe Theory and Practice - A Sourcebook, Hemisphere Publishing Corp., Washington, 1976.

2. Gernert, N., Sarraf, D., and Steinberg, M., "Flexible Heat Pipe Cold Plates for Aircraft Thermal Control," Aerospace Technology Conference and Exposition, SAE Paper No. 912105, Long Beach, CA, Sept. 23-26, 1991.

3. Steinberg, D.S., Vibration Analysis for Electronic Equipment, 2nd Edition, John Wiley & Sons, New York, 1988.

4. Gillingham, K.K., Plentizas, S., and Lewis, N.L., "G-Environments of F-4, F-5, F-15, and F-16 Aircraft During F-15 Tactics Development and Evaluation," USAFSAM-TR-85-51, July 1995 Final Report, Aerospace Medical Division (AFSC), Brooks AFB, TX 78235.

5. NASA GSFC Special Payloads Division, Experimenter Handbook: Getaway Special (GAS) Small Self-Contained Payloads, MD, 1989.

6. Richardson, J.W., Whitehurst, C.A., and Whitehouse, G.D., "Effect of Longitudinal Vibration on Heat Pipe Performance," J. Astronautical Sciences, Vol. 17, No. 5, March-April 1970, pp. 249-266.

7. Semena, M.G. and Nikolaenko, IU. E., "The Results of an Experimental Investigation of the Effect of Vibration Loading Parameters on the Working Characteristics of Heat Pipes," Energetika, January 1983, pp. 106-109.

8. Hou, Zengqi and Wen, Yaopu, "Heat Pipe Operating in a Spin Satellite," Proc. 6th IHPC Grenoble, France, May 25-29, 1987, pp. 439-442.

9. Kiseev, V.M., et al., J. of Engineering Physics, 50 (1986) 394.

10. Chelete, T.L., "Pilot Acceleration Training in the Egyptian Air Force," Proceedings IEEE NAECON, 1989, pp. 783-786.

11. Yerkes, K.L. and Brian, G.H., "Transient Response of Heat Pipes for Actuator Thermal Management," Paper No. 921024, 1992 SAE Aerospace Atlantic, Dayton, Ohio, April 7-10, 1992.

12. Yerkes, K.L., Chang, W.S., and Beam, J.E., "Heat Pipe Performance with Transient Heat Flux and Body Force Effects," Proc. 8th International Heat Pipe Conference, September

1992, Beijing, China. Advances in Heat Pipe Science and Technology, Ed. M Tongze, International Academic Publishers, Beijing, China 1993, pp. 205-213.

13. Ponnappan, R., Yerkes, K.L., Chang, W.S., and Beam, J.E., "Analysis and Testing of Heat Pipe in Accelerating Environment," Proc. 8th Intl. Heat Pipe Conference, Advances in Heat Pipe Science and Technology, Ed. Ma Tongze, International Academic Publishers, Beijing, China, 1993, pp. 250-255.

APPENDIX

DESIGN AND PERFORMANCE DETAILS OF THE FLEXIBLE HEAT PIPE

[Note: The nomenclature used here is as described in the text by S.W. Chi, Ref. 1]

A.1 WICKING HEIGHTS OF THE FLEXIBLE HEAT PIPE FOR WATER

This heat pipe uses sintered copper powder wick for the evaporator and flexible braided copper cable for artery wick. In order to determine the capillary pumping capacity of these wicks, capillary heights are calculated based on the wick materials data supplied by the fabricator. Table A-1 shows these results. According to the adverse tilt test on this pipe by Thermacore, the extrapolated 0W data at 60°C is 9.75 inches.

A.2 CAPILLARY LIMITS AND THE EFFECT OF "G"

Capillary pumping limits for this heat pipe are calculated both ways treating the sinter wick and the artery wick separately as the pumping wick for obtaining the maximum and minimum transport capacities. Table A-2 provides these results and the transport capacities are plotted in Figure A-1 and Figure A-2. Figure A-2 also shows the drop in capillary limit due to centrifugal acceleration which is calculated as follows:

Table A-1. Wicking Heights of Flexible Heat Pipe Wicks for Water

Temperature °C	Wicking Height, cm		
	Evaporator Wick (Sinter Copper) $r_{c_o}=1.59\times10^{-5}$ m	Cable Artery Wick	
		$r_{c_1}=3.06\times10^{-4}$ m	$r_{c_2}=0.554\times10^{-4}$ m
20	95.05	4.93	27.23
60	86.35	4.49	24.80
100	78.83	4.09	22.59
127	72.92	3.78	20.88
160	65.73	3.41	18.84
200	57.54	2.99	16.51
254	46.71	2.43	13.41

applicable equation: $$\rho_\ell g H = \frac{2\sigma_\ell}{r_c}\cos\theta$$

where,

r_{c_o} = 1.59×10^{-5} m (sinter copper)

r_{c_1} = 3.06×10^{-4} m (cable artery; measured)

r_{c_2} = 0.554×10^{-4} m (cable artery; based on adverse tilt test results supplied by Thermacore

θ = contact angle; assumed zero

H = wicking height

q = gravitational constant

ρ_ℓ, σ_ℓ = properties of water

Table A-2. Calculated Capillary Limits for Flexible Heat Pipe

Design Parameter	Temperature, °C						
	20	60	100	127	160	200	254
I. Evaporator Sinter Wick as the Pumping Wick: $r_{c_o} = 1.59 \times 10^{-5}$ m							
1. Ppm (N/m^2)	9308	8327	7409	6724	5862	4893	3670
2. ΔP_ℓ (N/m^2)	156	153	149	147	142	135	125
3. Pcm (N/m^2)	9152	8174	7260	6577	5720	4758	3545
4. $F_\ell L_{eff}$ ($N/m^2/W$)	48.83	24.21	15.46	12.84	10.77	9.893	9.49
5. Qcm (W)	187.4	337.6	469.6	512.2	531.1	484.0	373.6
II. Artery Cable as the Pumping Wick: $r_{c_2} = 0.554 \times 10^{-4}$ m							
1. Ppm (N/m^2)	2673	2391	2125	1926	1648	1402	1055
2. ΔP_ℓ (N/m^2)	63	62	60	59	57	54	50
3. Pcm (N/m^2)	2610	2329	2065	1867	1627	1348	1005
4. $F_\ell L_{eff}$ ($N/m^2/W$)	← Same as in Case I above →						
5. Q_{cm} (W)	53.5	96.2	133.6	145.0	151.0	137.0	106.0

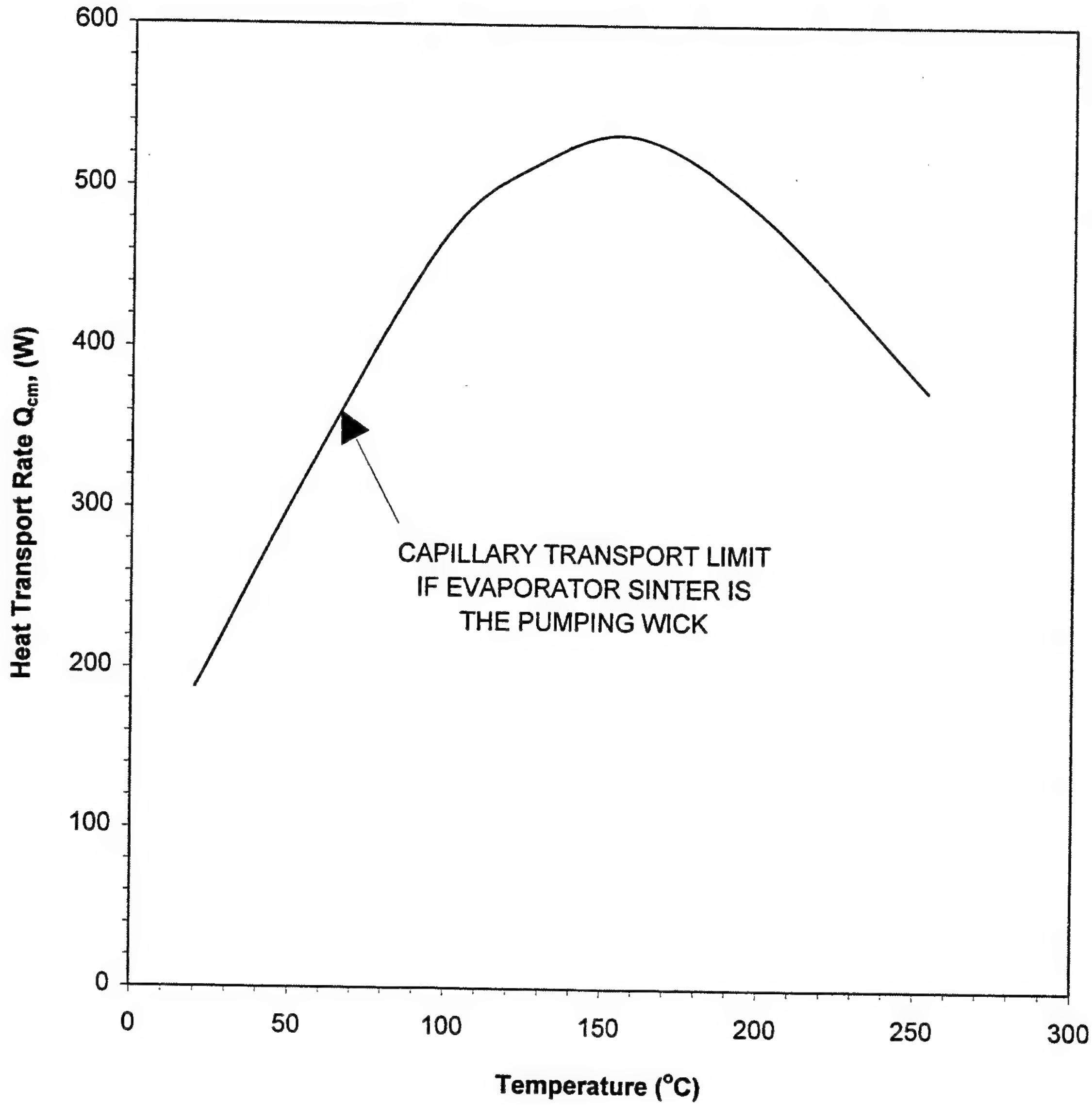

Figure A-1. Capillary Limit (Maximum)

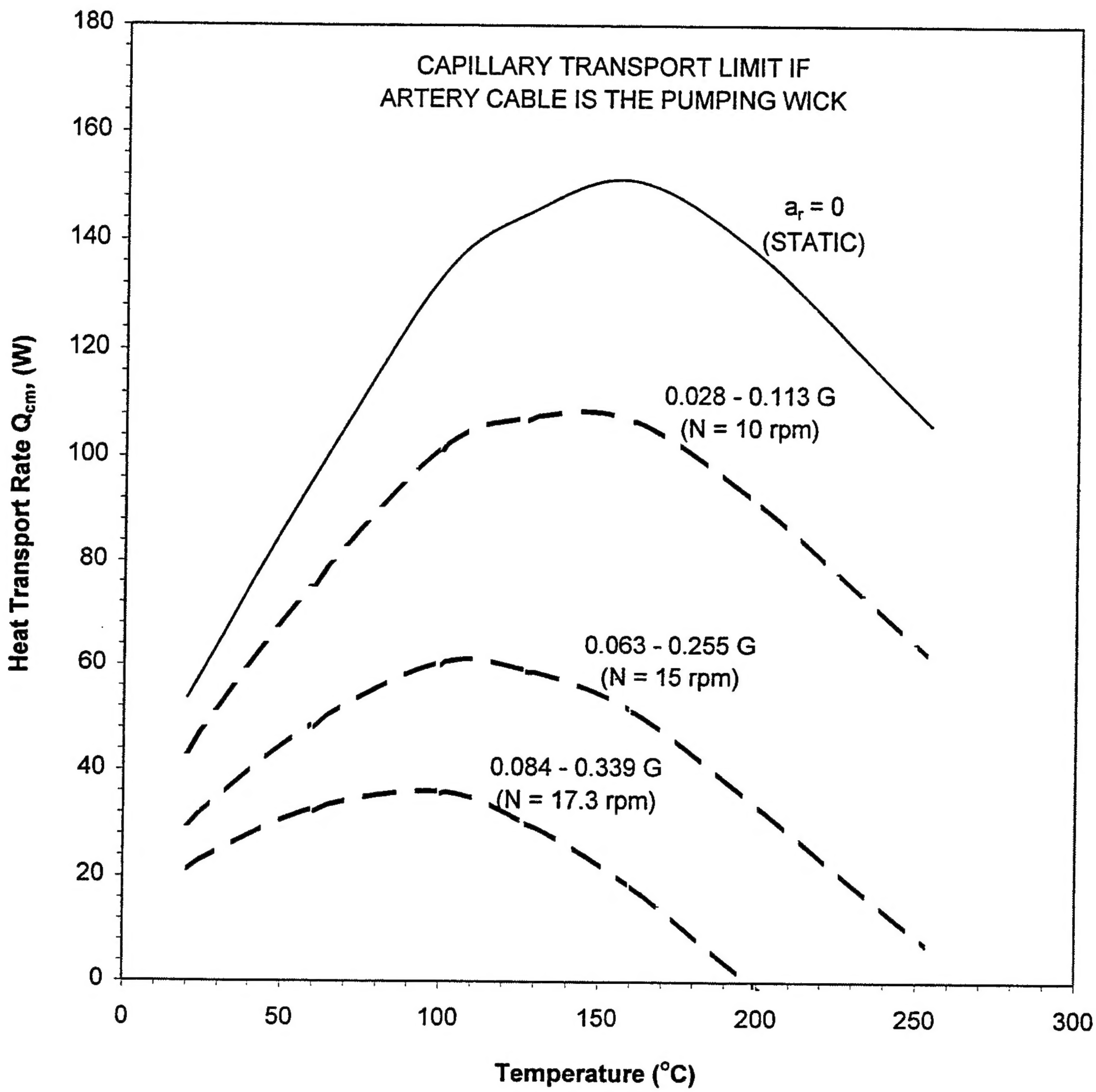

Figure A-2. Effect of G on Capillary Limit for Radial Mounting of Flexible Heat Pipe with $X_1 = 0.25$ m; $X_2 = 1.012$ m.

Effect of Radial G on Capillary Limit: Pressure exerted on the fluid element due to centrifugal acceleration, $X_2 = 1.012$ m; $X_1 = 0.25$ m.

$$P_{CA} = \int_{X_1}^{X_2} \rho_\ell \omega^2 x \, dx$$

$$= \rho_\ell \omega^2 \frac{\left(X_2^2 - X_1^2\right)}{2} = \rho_\ell \left(\frac{2\pi N}{60}\right)^2 \frac{\left(X_2^2 - X_1^2\right)}{2}$$

or

$$\boxed{P_{CA} = 0.0052728 \; \rho_\ell N^2}$$

Capillary limit with G-load} $Q_{CA} = \dfrac{P_{cm} - P_{CA}}{F_\ell L_{eff}} = \dfrac{P_{PM} - \Delta P_1 - P_{CA}}{F_\ell L_{eff}}$

Using the table of data calculated for static case, Q_{CA}, values are obtained for N = 10, 15, and 17.3 rpm as given in Table A-3.

Table A-3. Drop in Capillary Limit due to Centrifugal Acceleration for Radial Mounting

Temperature °C	Q_{CA}, [W]			Q_{CM} [W] Static
	10 rpm	15 rpm	17.3 rpm	
20	42.7	29.3	21.3	53.5
60	74.8	48.1	32.2	96.2
100	100.8	59.9	35.5	133.6
127	106.9	58.7	30.0	145.0
160	106.7	51.2	18.3	151.0
200	90.9	33.2	-	137.0
254	61.8	6.7	-	106.0

The Q_{CA} values in the table are plotted in Figure A-2.

NOMENCLATURE

a	acceleration, m/s^2
a_r	radial acceleration, m/s^2
a_R	transverse acceleration $\sqrt{a_r^2 + a_y^2}$, m/s^2
a_t	tangential acceleration, m/s^2
a_y	Vertical acceleration, m/s^2
Bo_1	Bond number for circumferential mounting
Bo_2	Bond number for radial mounting
d	diameter of artery cable, m
F_ℓ	liquid friction factor, N/m^2 per Wm
F_v	vapor friction factor, N/m^2 per Wm
g	gravitational constant, m/s^2
G	induced acceleration divided by "g", ND
K	permeability of wick, m^2
L	length of heat pipe, m
Q_o	heat transport, W
r	radius, m
r_c	capillary pore radius, m
T	temperature, °C
ΔT	temperature difference, °C

Greek Symbols

ϵ	wick porosity
θ	wetting angle
ρ_ℓ	liquid density, kg/m^3
ρ_v	vapor density, kg/m^3
σ	surface tension, N/m
ω	angular speed, rad/s
ψ	heat pipe inclination with respect to horizontal plane

NOMENCLATURE (CONT'D.)

Subscripts

c	condenser
AC	adiabatic to condenser
EA	evaporator to adiabatic